ARTICLE

Persistent microbiome alterations modulate the rate of post–dieting weight regain

Christoph A. Thaiss[1]*, Shlomik Itav[1]*, Daphna Rothschild[2,3]*, Mariska T. Meijer[1], Maayan Levy[1], Claudia Moresi[1], Lenka Dohnalová[1], Sofia Braverman[1], Shachar Rozin[1], Sergey Malitsky[4], Mally Dori-Bachash[1], Yael Kuperman[5], Inbal Biton[5], Arieh Gertler[6], Alon Harmelin[5], Hagit Shapiro[1], Zamir Halpern[7,8], Asaph Aharoni[4], Eran Segal[2,3]§ & Eran Elinav[1]§

In tackling the obesity pandemic, considerable efforts are devoted to the development of effective weight reduction strategies, yet many dieting individuals fail to maintain a long-term weight reduction, and instead undergo excessive weight regain cycles. The mechanisms driving recurrent post-dieting obesity remain largely elusive. Here we identify an intestinal microbiome signature that persists after successful dieting of obese mice and contributes to faster weight regain and metabolic aberrations upon re-exposure to obesity-promoting conditions. Faecal transfer experiments show that the accelerated weight regain phenotype can be transmitted to germ-free mice. We develop a machine-learning algorithm that enables personalized microbiome-based prediction of the extent of post-dieting weight regain. Additionally, we find that the microbiome contributes to diminished post-dieting flavonoid levels and reduced energy expenditure, and demonstrate that flavonoid-based 'post-biotic' intervention ameliorates excessive secondary weight gain. Together, our data highlight a possible microbiome contribution to accelerated post-dieting weight regain, and suggest that microbiome-targeting approaches may help to diagnose and treat this common disorder.

The past century has witnessed an alarming increase in the prevalence of obesity, with over 44% of the adult world population estimated to be overweight, and over 300 million adults suffering from morbid obesity. Obesity is considered a major risk factor for 'metabolic syndrome' and its complications, with consequences for life expectancy, quality of life and healthcare costs[1].

Despite continuous medical and scientific effort, long-term strategies aimed at attenuating or reversing the obesity epidemic have yielded disappointing results. While a plethora of dietary approaches efficiently induce weight reduction, in up to 80% of cases in which weight loss was initially successful, reduced weight is not maintained, and instead is followed by recurrent weight gain and relapsing metabolic complications within 12 months of initial weight reduction that may even exceed the pre-dieting metabolic derangements[2]. Post-dieting weight regain is substantially influenced by non-genetic factors, as exemplified by progressively worsening weight regain in weight-cycling twins as compared to their non-dieting siblings[3], and is suggested to be independent of starting weight[4] and level of exercise[5]. Thus, the mechanisms underlying the weight-cycling-induced obesity phenomenon, commonly referred to as the 'yo-yo effect', remain to be determined[6,7].

An emerging factor affecting human metabolic homeostasis and the risk for obesity and its metabolic complications is the intestinal microbiome. Compositional and functional microbiome alterations, termed dysbiosis, have been suggested to contribute to the pathogenesis of obesity in both animal models and humans[8,9]. Moreover, dietary changes have been demonstrated to be central drivers of microbiome composition and function, and markedly affect the microbiome within days of initiation[10,11].

In this study, we used mouse models of weight loss and recurrent obesity to investigate the mechanisms underlying exacerbated

metabolic complications following weight cycling. We find that, in contrast to obesity-associated metabolic derangements that can be efficiently reverted upon dieting, obesity-induced alterations to the microbiome persist over long periods of time and enhance the rate of weight regain upon encounter of a second metabolic challenge. This post-dieting dysbiosis affects intestinal flavonoid levels, which, in turn, may impact host energy expenditure. We further devise a machine-learning algorithm that successfully predicts the personalized propensity for recurrent diet-induced obesity solely on the basis of microbiome composition and demonstrate that faecal microbiome transplantation (FMT) or metabolite-based treatment may ameliorate exacerbated post-dieting weight regain.

Enhanced weight regain after dieting

To study the mechanisms modulating post-dieting weight regain, we used a mouse model of recurrent obesity, in which mice were exposed to cycles of a high-fat diet (HFD), interleaved by normal chow (NC) consumption (cycHFD, Fig. 1a). Consequently, in these mice, weight gain and metabolic syndrome developed during primary exposure to HFD, followed by recuperation and weight reduction during exposure to NC, and then by re-emergence of weight gain and associated metabolic disturbances in subsequent HFD-mediated obesity cycles. As controls, we used mice continuously fed a HFD, mice continuously fed a NC diet, and mice that were exposed to only a single cycle of HFD (primHFD, Fig. 1a). As observed in recurrently dieting humans[2], a preceding obesity–weight-loss cycle rendered mice susceptible to accelerated secondary weight gain, even after fully returning to baseline weight (Fig. 1b, c and Extended Data Fig. 1a, b). As a result, the net weight gain, that is, the weight induced during identical durations of high-fat feeding, was higher in the weight-cycling group compared to

[1]Immunology Department, Weizmann Institute of Science, 76100 Rehovot, Israel. [2]Department of Computer Science and Applied Mathematics, Weizmann Institute of Science, 76100 Rehovot, Israel. [3]Department of Molecular Cell Biology, Weizmann Institute of Science, 76100 Rehovot, Israel. [4]Department of Plant and Environmental Sciences, Weizmann Institute of Science, 76100 Rehovot, Israel. [5]Department of Veterinary Resources, Weizmann Institute of Science, 76100 Rehovot, Israel. [6]The Robert H. Smith Faculty of Agriculture, Food and Environment, The Hebrew University, Rehovot 76100, Israel. [7]Research Center for Digestive Tract and Liver Diseases, Tel Aviv Sourasky Medical Center, Sackler Faculty of Medicine, Tel Aviv University, 69978 Tel Aviv, Israel. [8]Digestive Center, Tel Aviv Sourasky Medical Center, 64239 Tel Aviv, Israel.
*These authors contributed equally to this work.
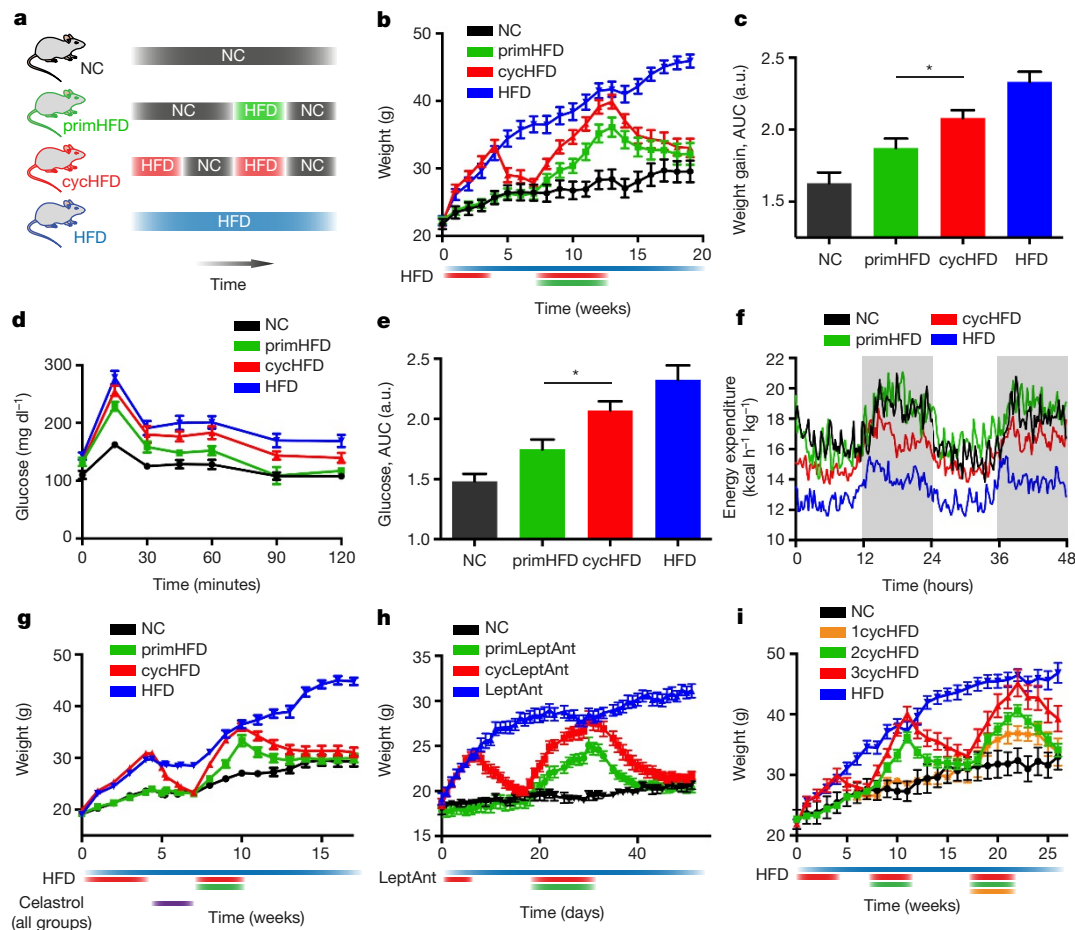§These authors jointly supervised this work.

Figure 1 | Enhanced recurrent weight gain after treatment of obesity.
a–**c**, Schematic (**a**), weight curves (**b**), and weight regain quantification (**c**) of mice undergoing weight cycling and controls. a.u., arbitrary units.
d–**f**, Glucose levels after glucose tolerance test (**d**), glucose quantification (**e**) and energy expenditure over 48 h (**f**) during weight regain (week 10).

g–**i**, Recurrent weight gain in mice treated with celastrol (**g**), leptin antagonist (LeptAnt; **h**), or up to three HFD cycles (**i**). Coloured bars below weight curves depict durations of the indicated treatments. Experiments were repeated at least twice. Data are mean ± s.e.m. *$P < 0.05$ by ANOVA. See Supplementary Tables 5 and 6 for exact n and P values.

mice continuously fed a HFD (Extended Data Fig. 1c). The maximal weight reached by both weight-cycling and continuous HFD groups was comparable, and higher than in mice exposed to a first cycle of HFD (Fig. 1b). Moreover, as compared to mice exposed to a single cycle of HFD, recurrent obesity was characterized by a significant increase in total body fat as determined by MRI (Extended Data Fig. 1d, e), enhanced glucose intolerance (Fig. 1d, e), and elevated serum levels of leptin and low-density lipoprotein (LDL), but not high-density lipoprotein (HDL) (Extended Data Fig. 1f–h). Accelerated weight regain in post-dieting mice was associated with decreased energy expenditure (Fig. 1f and Extended Data Fig. 1i–p), while food intake remained unaffected (Extended Data Fig. 1q).

Similarly, exacerbated metabolic derangements following a weight gain/weight reduction cycle were observed when weight loss was pharmacologically accelerated by celastrol, a quinone methide recently found to induce weight loss[12] (Extended Data Fig. 2a, b). Upon reinstatement of HFD, mice developed significantly exacerbated secondary weight gain (Fig. 1g, Extended Data Fig. 2c–e), as compared to celastrol-treated controls without preceding obesity. Furthermore, to model recurrent obesity induced by hyperphagia rather than dietary composition, we pharmacologically inhibited leptin signalling[13,14]. Mice administered a leptin antagonist for one week while consuming NC significantly gained weight, and fully returned to normal weight upon cessation of leptin antagonist treatment (Fig. 1h). Upon a second challenge with the leptin antagonist, these mice featured a more pronounced weight regain compared to mice administered the leptin antagonist for the first time (Fig. 1h and Extended Data Fig. 2f, g).

When exposed to a third cycle of HFD-induced obesity, weight-cycling mice exhibited a further exacerbation in weight gain (Fig. 1i), obesity (Extended Data Fig. 2h), and dyslipidemia (Extended Data Fig. 2i) as compared to control animals experiencing secondary or primary weight-gain cycles. Together, these experiments suggest that previous obesity–dieting cycles progressively enhance the susceptibility to accelerated weight regain and associated metabolic complications.

Persistence of post-dieting microbiome alterations

Given the above results, we proposed that initial obesity had caused persistent abnormalities that predisposed mice to relapsing metabolic disease upon re-feeding with HFD. We therefore performed metabolic profiling during the first episode of obesity (Extended Data Fig. 2j) and at the 'nadir' phase (Extended Data Fig. 3a), that is, when previously obese mice had returned to normal weight that was indistinguishable from that of NC-fed controls. Despite marked metabolic derangements during the primary obesity phase (Extended Data Fig. 2k–o), neither body fat content, serum cholesterol, glucose tolerance, nor serum insulin levels were significantly different between post-dieting mice and their non-cycling controls during the nadir post-obesity phase (Extended Data Fig. 3b–f). Similarly, other hallmarks of obesity, such as oxygen consumption, energy expenditure, physical activity, as well as food and drink intake fully returned to normal baseline levels upon weight loss during the nadir phase (Extended Data Fig. 3g–l and Extended Data Fig. 4a–l).

In contrast, the composition of the intestinal microbiota, which had assumed a dysbiotic state during the primary obesity phase,
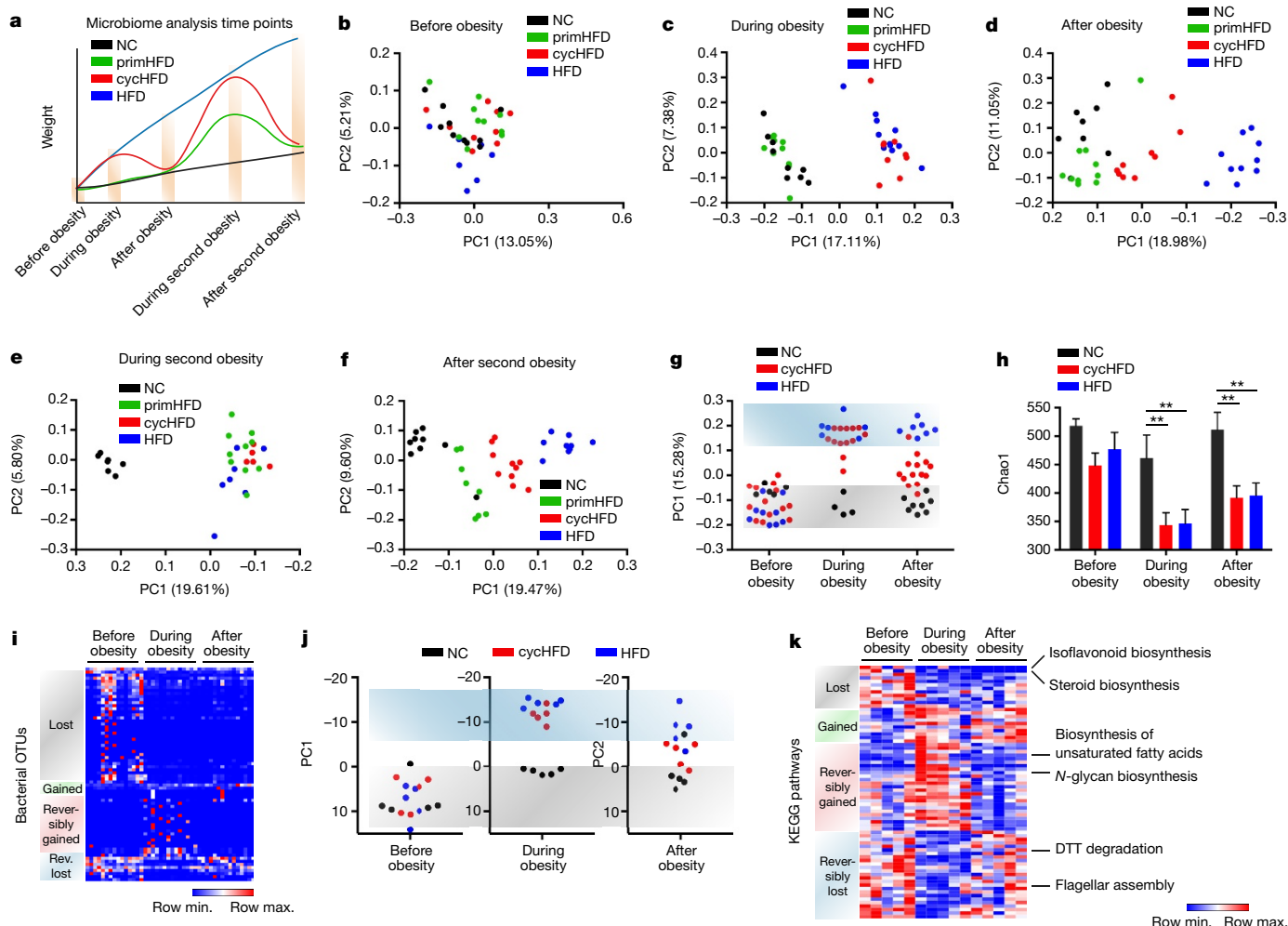
Figure 2 | Persistent microbiome alterations after weight loss.
a, Schematic of sampling times for microbiota analysis. **b–f**, Principal coordinate analyses (PCoA) of unweighted UniFrac distances of microbiota composition at the indicated time points. **g–i**, PCoA (**g**), alpha diversity (**h**), and OTU heatmap (**i**) of weight-cycling mice and controls before, during, and after obesity. **j, k**, Principal component analysis (PCA; **j**) and heatmap (**k**) of bacterial KEGG pathways in weight-cycling mice and controls. Experiments were repeated twice. Data are mean ± s.e.m. **$P < 0.01$ by ANOVA. See Supplementary Tables 5 and 6 for exact n and P values.

did not return to its original composition at the time of post-dieting weight and metabolic normalization (Fig. 2a–d and Extended Data Fig. 5a). Instead, the microbiota assumed an intermediate configuration between the dysbiotic and normal states (Fig. 2d and Extended Data Fig. 5a). A similar microbiome configuration shift was observed after recovery from a second cycle of recurrent obesity (Fig. 2e, f and Extended Data Fig. 5a). We confirmed these findings by targeting an alternative region of the 16S locus for amplicon sequencing (Extended Data Fig. 5b–d). Notably, in addition to the significant alteration in bacterial composition persisting after metabolic normalization (Fig. 2g), bacterial alpha diversity was reduced during the obese state and did not recover upon return to normal weight and metabolic homeostasis (Fig. 2h). To determine the operational taxonomic units (OTUs) that remained altered after dieting, we normalized the OTU abundance of weight cycling mice to age-matched NC controls and classified the OTUs according to their temporal behaviour. Notably, only 45% of all OTUs returned to pre-obesity levels after dieting (Fig. 2i and Extended Data Fig. 5e, f), while obesity-induced effects on the microbiome persisted in multiple bacterial taxa (Extended Data Fig. 5g–l). Similarly, persistent post-obesity microbiota alterations in composition and alpha diversity were noted in mice in which weight loss had been aided with celastrol treatment (Extended Data Fig. 5j–m).

To determine the functional consequences of this incomplete post-dieting microbiota recovery, we performed shotgun metagenomic

sequencing and normalized the temporal behaviour of gene abundances to NC controls. We identified 773 bacterial genes whose abundance was altered by HFD and did not return to control levels after dieting (Extended Data Fig. 6a–c). Likewise, microbial functionalities did not fully recover in previously dieting mice, both at the level of gene modules (Extended Data Fig. 6d) and functional pathways (Fig. 2j). Similar to OTUs, reversal of obesity led only to a partial recovery of microbial functions (Extended Data Fig. 6e–h), with multiple obesity-induced microbiome aberrations persisting during weight loss (Fig. 2k). Abundances of genes from multiple metabolic pathways, including isoflavonoid and steroid biosynthesis, were reduced during high-fat feeding and did not recover upon dieting (Extended Data Fig. 6i, j). Collectively, these data indicate that reversal of obesity by dieting results in a microbiome configuration that remains altered, as compared to control mice without prior obesity, even when a state of metabolic normalization is reached.

The post–dieting microbiome contributes to weight regain

We next sought to investigate whether the persistent post-obesity microbiome signature was causally involved in the metabolic complications associated with recurrent weight gain. To this end, we treated mice with broad-spectrum antibiotics during the post-obesity weight loss period (Fig. 3a). Expectedly, antibiotic treatment during dieting
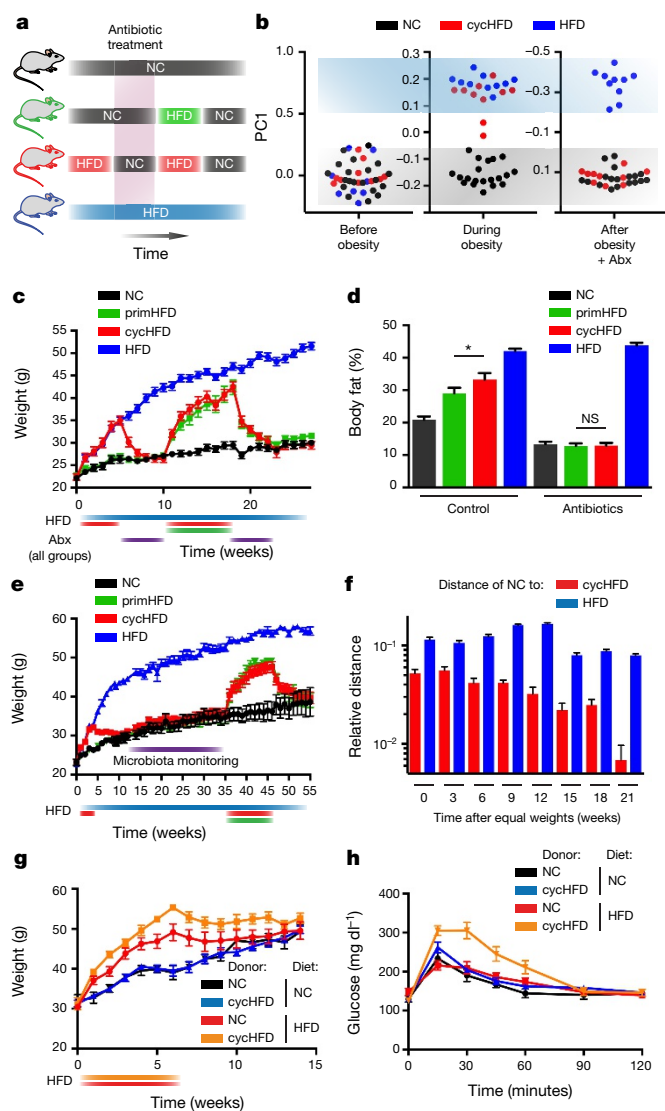
Figure 3 | Post-dieting microbiome alterations drive exacerbated weight regain. a, Schematic of microbiota equilibration by antibiotics during weight loss. **b–d**, PCoA of faecal microbiota (**b**), weight curve (**c**) and body fat content (**d**) during weight regain of weight-cycling mice undergoing antibiotic (Abx) treatment during weight loss. **e**, Weight curve of mice monitored for microbiota equilibration after dieting before induction of secondary obesity. **f**, Microbial dissimilarity expressed as differential UniFrac distance over time between cycHFD and HFD mice compared to NC controls. **g**, **h**, Weight curve (**g**) and glucose levels after glucose tolerance test (**h**) in germ-free recipients one week after microbiota transfer from cycHFD and NC mice. Experiments were repeated twice. Data are mean ± s.e.m. *$P < 0.05$ by ANOVA; NS, not significant. See Supplementary Tables 5 and 6 for exact n and P values.

abolished the post-obesity microbiome signature and equilibrated the microbiota composition and alpha diversity between previously obese mice and controls, while the microbiota of untreated mice maintained an intermediate configuration (Fig. 3b and Extended Data Fig. 7a, b). Remarkably, antibiotic treatment also abrogated the exacerbation of metabolic derangements upon re-exposure to a HFD, including weight gain, body fat content and glucose intolerance, as compared to untreated weight-cycling mice (Fig. 3c, d and Extended Data Fig. 7c–e).

We next determined the time required for spontaneous reversal of the persistent post-dieting microbiome alterations. To this end, we monitored the microbiota composition every three weeks upon return of previously obese mice to phenotypic normality (Fig. 3e). Notably,

spontaneous reversion of the post-cycling microbiota composition back to NC configuration was achieved only 21 weeks after the completion of successful dieting, that is, a time period more than five times longer than the initial weight gain or dieting period (Fig. 3f and Extended Data Fig. 7f–h). The return to compositional normality in the post-obesity microbiota was associated with gradual acquisition or loss of bacterial taxa (Extended Data Fig. 7i–k). Importantly, following the spontaneous microbiota equilibration, re-exposure to a HFD resulted in an indistinguishable weight gain of formerly obese mice compared to the primary weight gain of HFD-fed mice (Fig. 3e and Extended Data Fig. 7l).

Additionally, we performed faecal transfer experiments, in which the microbiota from previously obese mice (cycHFD) and from phenotypically identical controls (NC) were transferred to germ-free mice, which were subsequently fed either NC or a HFD (Extended Data Fig. 8a). The compositional differences between the microbiota from formerly weight-cycling mice and controls persisted in germ-free recipients (Extended Data Fig. 8b–d). Notably, under NC conditions, naive and post-cycling microbiome-transplanted germ-free mice featured similar weight and glucose tolerance (Fig. 3g, h and Extended Data Fig. 8e, f), suggesting that the post-obesity microbiome did not feature intrinsic obesogenic properties. In contrast, when fed a HFD, recipients of post-weight cycling microbiota exhibited significantly enhanced weight gain and glucose intolerance as early as one week after faecal transplantation, as compared to recipients of microbiome from NC-consuming mice (Fig. 3g, h and Extended Data Fig. 8e, f). Thus, enhanced metabolic derangements in cycling microbiome-transplanted HFD-fed germ-free mice developed even in the absence of previous bouts of obesity in recipient mice, indicating that the post-dieting microbiome configuration coupled with a secondary obesogenic challenge suffices to induce an enhanced metabolic phenotype. Together, these data suggest that the post-dieting microbiota contributes to the susceptibility to develop aggravated metabolic complications upon re-exposure to obesity-inducing conditions.

Microbiota composition predicts weight regain

Given the above causal connection between microbiome configuration and post-dieting weight regain, we asked whether the extent of recurrent weight gain could be computationally predicted for each individual mouse based on its microbiota composition at the post-dieting nadir period. We therefore profiled the microbiota composition of 25 mice that had undergone post-obesity dieting until metabolic normality and 25 weight-matched NC controls (Fig. 4a). We first devised a machine-learning algorithm, based solely on the microbiota composition, aimed at predicting a history of obesity or lack thereof (Fig. 4a, see Methods). Notably, the derived random forest classifier predicted obesity history nearly perfectly (AUC = 0.96, Fig. 4b).

We then attempted to predict the exact extent of weight regain of each mouse upon secondary exposure to HFD, based on the mouse's post-dieting microbiome configuration. Prediction solely on the basis of obesity history (that is, without any machine learning model employed) yielded a low prediction accuracy ($R = 0.21$, Extended Data Fig. 8g). By contrast, a 16S rDNA-based prediction using a leave-one-out cross-validation scheme performed significantly better ($R = 0.58$, Extended Data Fig. 8h). Notably, a two-step microbiome-based algorithm that first predicts obesity history and then predicts weight regain on the basis of the predicted history, achieved a highly accurate prediction of the extent of weight regain across individual mice ($R = 0.72$, Fig. 4c).

To determine which features of the microbiota contribute to the algorithm's ability to predict the degree of weight gain, we ranked all OTUs detected in the faecal microbiomes according to feature importance for prediction (Fig. 4d). Notably, a total of 189 OTUs contributed to the algorithm's predictions and the magnitude of their contributions displayed a continuum with no OTU standing out as a major contributor (Fig. 4e). This suggests that the composition of the commensal
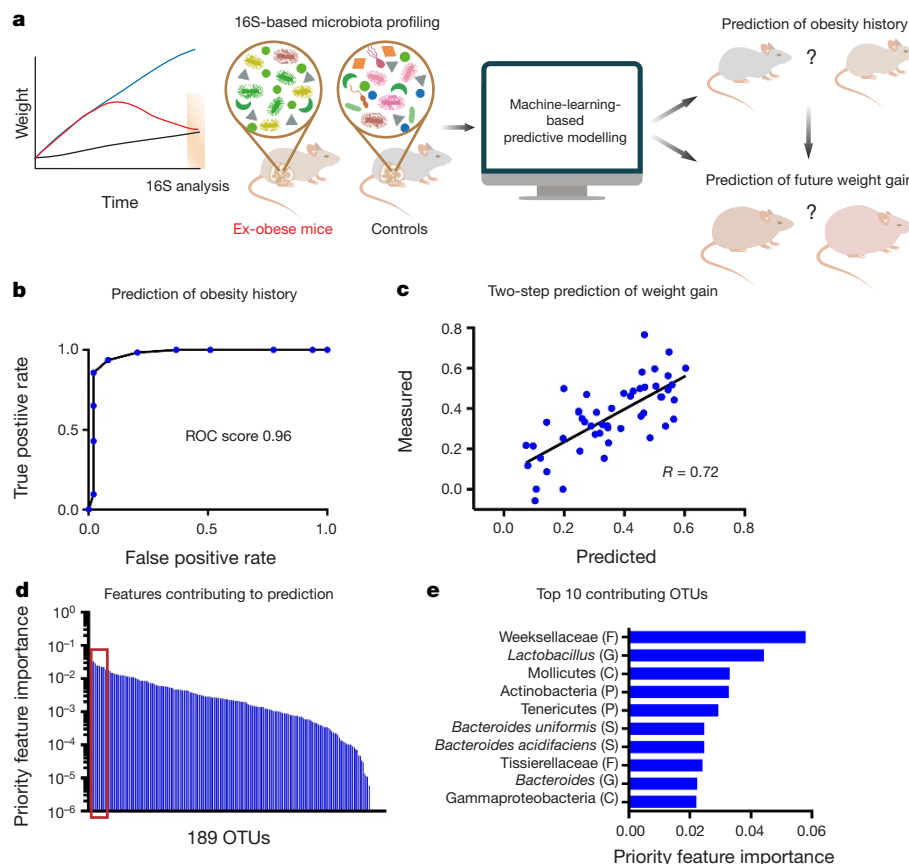
Figure 4 | Accurate prediction of post-dieting weight regain by microbiota features. a, Schematic of microbiota-based prediction of weight-gain history and weight regain upon HFD feeding. **b, c**, Prediction of prior obesity (**b**) and weight regain (**c**) based on 16S data. **d**, Ranked list of OTUs contributing to algorithm-based weight prediction. **e**, List of ten most important OTUs from **d**. Letters in brackets indicate taxonomic level (F, family; G, genus; C, class; P, phylum; S, species). See Supplementary Table 5 for exact *n* values.

bacteria as a whole, rather than a small subset of species, drives the post-dieting microbiome alterations that contribute to the susceptibility to relapsing obesity. Together, these results indicate that the microbiota configuration may be used to predict the history of HFD-induced obesity in mice as well as the extent of personalized weight regain that occurs upon recurrence of similar obesity-inducing conditions.

Metabolites contribute to post–dieting weight regain

We next determined whether microbiome modulation during the post-weight-cycling period could ameliorate the extent of secondary weight gain and its metabolic complications. To this end, we performed daily faecal microbiome transplantation (FMT) for 4 weeks, using 'naive' or post-dieting donor microbiomes transferred into colonized weight-cycling mice during the nadir post-dieting period (Fig. 5a). Upon transplantation, compositional differences between the microbiota from formerly weight-cycling mice and controls persisted in the corresponding FMT recipients (Extended Data Fig. 8i–k). Notably, recipients of a non-cycling 'healthy' microbiome during the nadir post-obese period exhibited an ameliorated secondary weight gain (Fig. 5b and Extended Data Fig. 8l, m), reduced glucose intolerance (Fig. 5c and Extended Data Fig. 8n), decreased body fat (Fig. 5d, e), and increased lean mass (Extended Data Fig. 8o) as compared to mice undergoing a control FMT with a post-cycling microbiome. These results indicate that restoration of normal microbiota function after dieting may prevent exacerbation of metabolic derangements upon weight regain.

Given the effectiveness of FMT, we sought to gain further insight into how microbiota replenishment ameliorates the propensity for recurrent obesity after weight loss. To this end, we longitudinally compared the faecal metabolomics profiles between mice undergoing HFD-induced weight-cycling and control NC-fed mice. We normalized the metabolite levels in weight-cycling mice to those of age-matched NC controls at each time point and then classified each metabolite according to temporal patterns. As expected, HFD induced major alterations in the faecal metabolome, which were partially reversed upon subsequent weight loss (Fig. 5f, g and Extended Data Fig. 9a–d). However, in nearly half of all metabolites altered by HFD, including several bile acids, the obesity-induced changes persisted after return to phenotypic normality (Fig. 5f, g and Extended Data Fig. 9e–h).

Among the metabolites most significantly depleted by HFD whose levels did not recover upon regain of metabolic health were the dietary flavonoids apigenin and naringenin (Fig. 5f–i). Both compounds remained suppressed for as long as 15 weeks after weight normalization (Fig. 5h, i). Flavonoids are commonly ingested diet-derived compounds that are metabolized by the intestinal microbiota[15]. The microbiome contribution to intestinal flavonoid levels was evident from the elevated levels of apigenin and naringenin in antibiotics-treated or germ-free mice (Fig. 5j). We therefore hypothesized that a combination of dietary flavonoid availability and microbiome-mediated flavonoid-degrading capacity may contribute to the total intestinal flavonoid pool. To this end, we followed the kinetics of flavonoids, the flavonoid-biosynthetic enzyme chalcone synthase and the flavonoid-degrading enzyme flavanone 4-reductase (Extended Data Fig. 9i and Supplementary Table 1), over the course of an obesity/weight loss/weight regain cycle (Extended Data Fig. 10a).

During primary obesity, low intestinal flavonoid levels (Fig. 5h, i) were contributed to by low flavonoid availability in the HFD (Extended Data Fig. 10b) coupled to a microbiome shift towards a flavonoid-degrading configuration, as evident by the increase in flavanone 4-reductase levels, and no similar increase in the level of chalcone synthase (Extended Data Fig. 10c, d). During induction of weight loss by
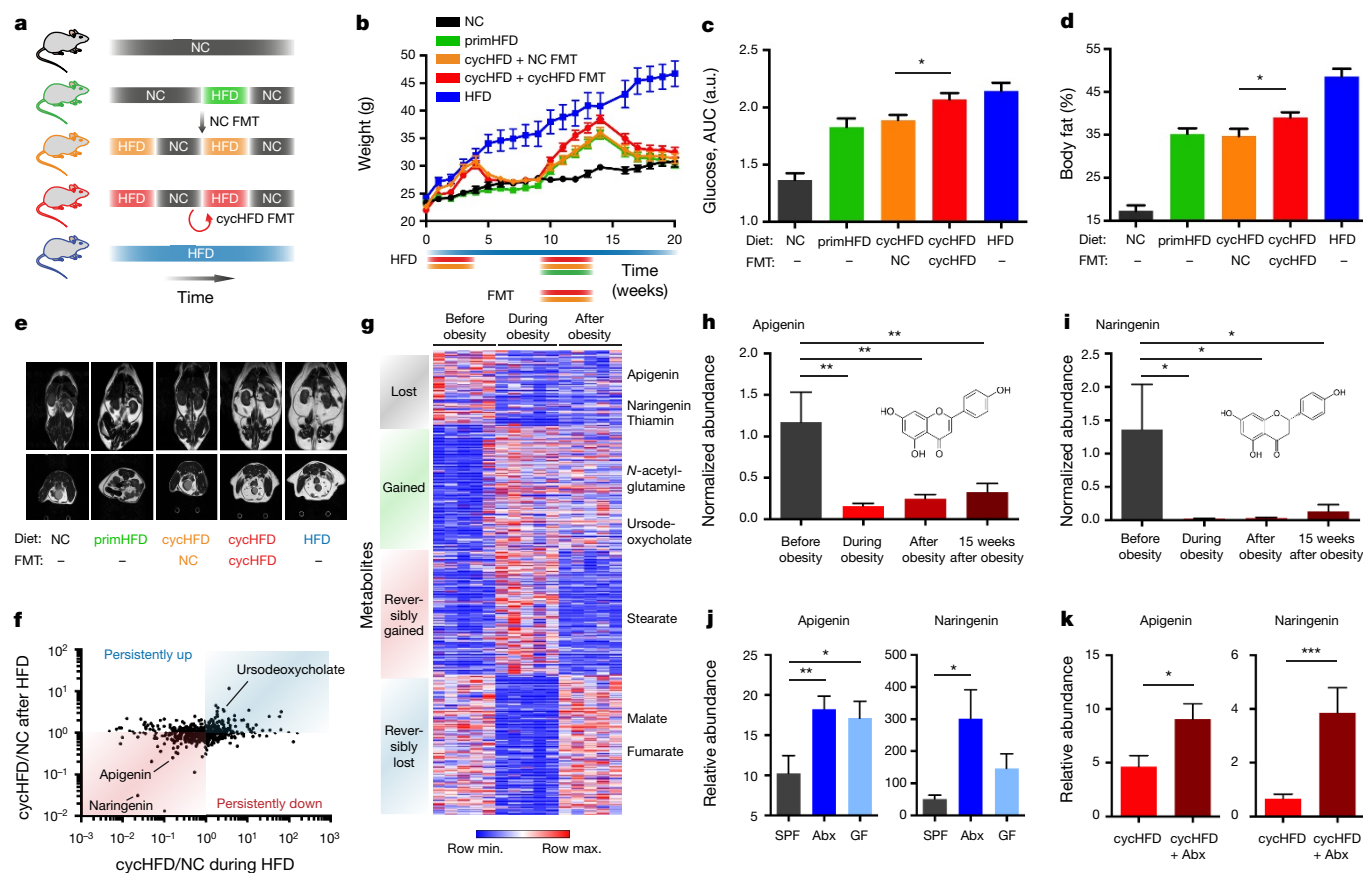
Figure 5 | Microbiome modulation ameliorates post-dieting weight regain. a–e, Schematic (**a**), weight curve (**b**), glucose level quantification after glucose tolerance test (**c**), body fat content (**d**), and representative MRI scans (**e**) during weight regain of weight-cycling mice undergoing faecal microbiota transplantation (FMT). **f, g,** Relative abundances (**f**) and heatmap (**g**) of intestinal metabolites before, during, and after obesity. **h–k,** Normalized intestinal abundances of apigenin and naringenin before,

during, and after obesity, as well as 15 weeks after successful dieting (**h, i**), in antibiotic-treated (Abx), germ-free (GF), and specific-pathogen-free (SPF) mice (**j**), and in mice treated with antibiotics during weight loss (**k**). Experiments were repeated twice. Data are mean ± s.e.m. *$P < 0.05$, **$P < 0.01$, ***$P < 0.001$ by ANOVA (**c–j**) or Mann–Whitney U-test (**k**). See Supplementary Tables 5 and 6 for exact n and P values.

reversion to a NC diet, dietary flavonoid availability returned to its normally high level (Extended Data Fig. 10b) yet intestinal flavonoid levels remained persistently low, including those of naringenin-derived eriodictyol (Fig. 5h, i and Extended Data Fig. 10e). At this nadir phase, the flavonoid-degrading microbiome contributed to the persistently low flavonoid levels, as suggested by elevated levels of flavanone 4-reductase (Extended Data Fig. 10c) and by the effect of antibiotic treatment during the weight-reduction phase, which diminished the levels of flavonone 4-reductase (Extended Data Fig. 10f) and normalized flavonoid levels (Fig. 5k). Upon acute secondary induction of obesity (Extended Data Fig. 10g), the combination of low dietary flavonoid availability (Extended Data Fig. 10b), coupled with the long-standing presence of a flavonoid-degrading microbiome and associated low flavonoid levels, probably contributed to reduced flavonoid levels in weight-cycling mice as compared to controls undergoing primary weight gain (Extended Data Fig. 10h, i).

Apigenin and naringenin have been reported to affect food intake, adipocyte differentiation, and lipid metabolism[16–18]. We therefore hypothesized that, similarly to FMT-induced restoration of a naive flavonoid-degrading microbiome in weight-cycling mice, direct flavonoid replenishment in these mice may ameliorate the exacerbated relapsing obesity phenotype. Indeed, oral daily administration of both flavonoids to post-dieting mice during the post dieting nadir and secondary weight regain period (Fig. 6a) resulted in normalization of intestinal apigenin and naringenin levels to control levels (Extended Data Fig. 10j), with no effect noted on microbiome composition (Extended Data Fig. 10k). Similar to FMT, combined flavonoid

treatment ameliorated the rate of secondary weight regain (Fig. 6b, c and Extended Data Fig. 10l, m). Together, these results suggest that low apigenin and naringenin levels in post-dieting mice contribute to an exacerbated weight regain, while their therapeutic replenishment ameliorates this susceptibility.

Flavonoids modulate weight regain and UCP1 expression

To investigate possible mechanisms by which apigenin and naringenin ameliorate recurrent post-dieting obesity, we measured metabolic and behavioural parameters in flavonoid-administered weight-cycling mice, as compared to untreated weight-cycling mice. Notably, weight-adjusted energy expenditure was markedly reduced in weight-cycling mice (Fig. 6d–f and Extended Data Fig. 11a–f), but was normalized upon flavonoid administration (Fig. 6d–f and Extended Data Fig. 11a–f), suggesting that apigenin and naringenin might impact host energy expenditure. Of note, a similar effect of flavonoids on weight management was observed in previous studies[19], while the link between flavonoid supplementation and enhanced energy expenditure was reached only upon normalization of energy expenditure to body weight. Other metabolic parameters were not affected by flavonoid treatment (Extended Data Fig. 11g, h and Extended Data Fig. 12a–f). Similarly, mice treated with antibiotics during the nadir period featured enhanced energy expenditure upon re-administration of HFD (Fig. 6g, Extended Data Fig. 12g–l and Extended Data Fig. 13a–c), in line with higher levels of flavonoids (Fig. 5k) and amelioration of the exacerbated weight regain (Fig. 3c), while not altering other metabolic parameters during recurrent weight gain (Extended Data Fig. 13d–l).
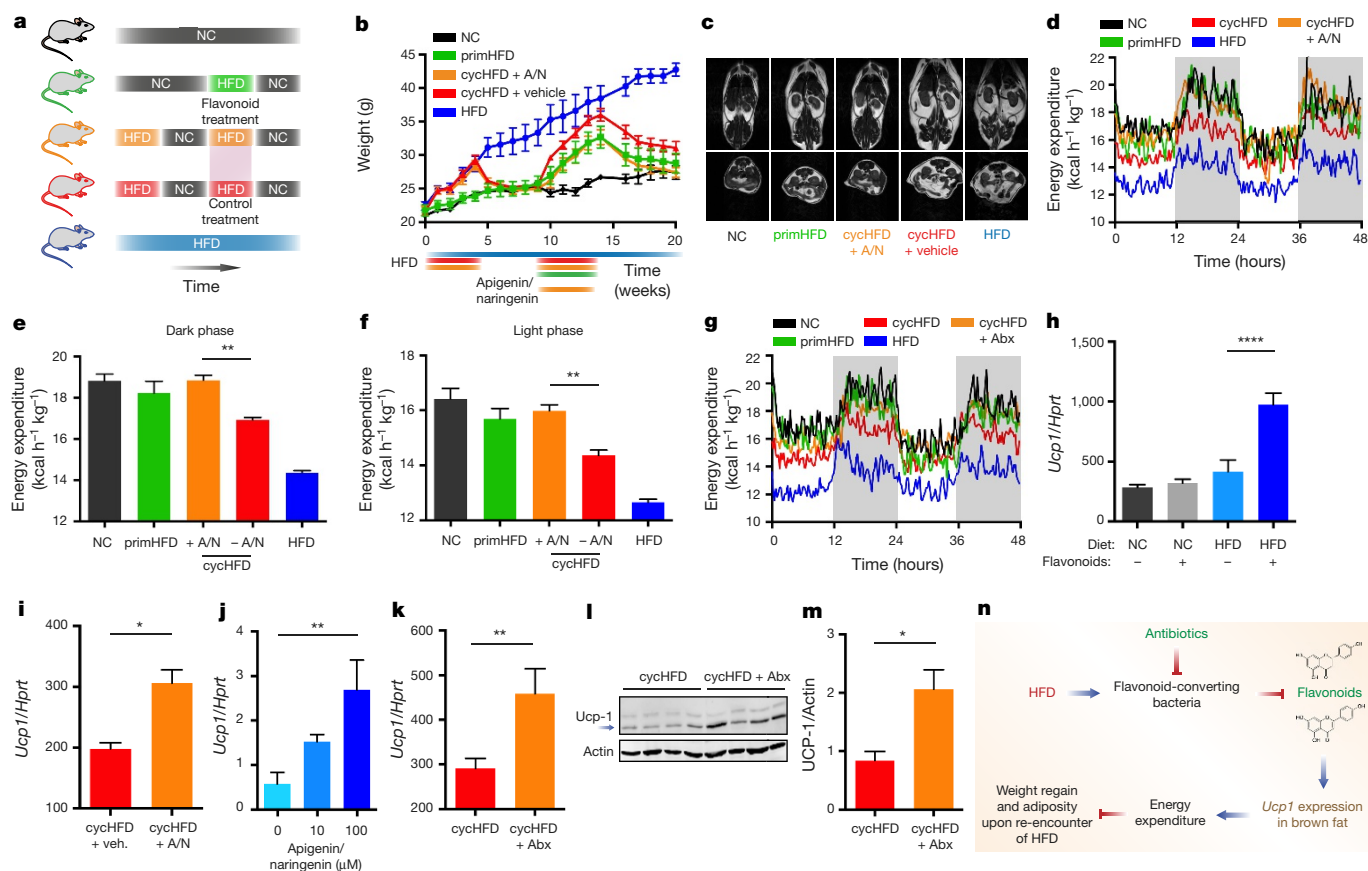
Figure 6 | Metabolite modulation ameliorates post-dieting weight regain. a–f, Schematic (**a**), weight curve (**b**), representative MRI scans (**c**), representative energy expenditure recording (**d**), and quantifications during the dark phase (night) (**e**) and light phase (day) (**f**) of weight-cycling mice with or without supplementation of apigenin and naringenin (A/N) during weight regain. **g**, Energy expenditure recording during weight regain of weight-cycling mice with or without antibiotic treatment before weight regain. **h–m**, Brown adipose tissue (BAT) *Ucp1* transcript (**h–k**) or UCP1 protein (**l–m**) levels in mice on HFD or NC receiving A/N

or vehicle by daily gavage for 2 weeks (**h**), in weight-cycling mice with or without A/N treatment during weight regain (**i**), in BAT explants cultured with A/N for 24 h (**j**), and in mice during weight regain after antibiotic treatment during weight loss (**k–m**). **n**, Model of diet–microbiota–energy-expenditure interactions during dieting and weight regain. Experiments were repeated twice. Data are mean ± s.e.m. *$P < 0.05$, **$P < 0.01$, ****$P < 0.0001$ by ANOVA (**e, f, h, j**) or Mann–Whitney U-test (**i, k, m**). See Supplementary Tables 5 and 6 for exact n and P values.

Finally, we pursued possible mechanisms by which flavonoids may participate in the regulation of host energy expenditure. Since brown adipose tissue (BAT) is a major regulator of thermogenesis in mammals, and since other members of the flavonoid family have been previously associated with the induction of the major thermogenic factor uncoupling protein 1 (UCP1)[20–22], we analysed *Ucp1* expression in mice fed NC or HFD and orally administered with apigenin and naringenin. As early as two weeks after the start of flavonoid treatment, *Ucp1* transcript levels were significantly elevated in the BAT of mice fed a HFD, but not in those fed NC (Fig. 6h). Likewise, *Ucp1* expression was elevated in weight-cycling mice upon apigenin and naringenin supplementation during the HFD-induced weight-regain period (Fig. 6i). *Ucp1* was also induced by flavonoids in BAT explants in a concentration-dependent manner (Fig. 6j), suggesting that there exists a direct effect of apigenin and naringenin on the modulation of gene expression in BAT. Given that antibiotic treatment elevated intestinal flavonoid levels (Fig. 5k) and host energy expenditure (Fig. 6g and Extended Data Fig. 12h, l), we determined the levels of UCP1 in the BAT of antibiotic-treated weight-cycling mice. Indeed, we found both transcript and protein levels of UCP1 to be elevated in the group receiving antibiotics (Fig. 6k–m), providing a potential mechanistic explanation for recent observations of *Ucp1* induction in germ-free mice[23].

Taken together, these associations suggest a model in which HFD promotes the growth of flavonoid-metabolizing bacteria, which in turn decrease the amount of bioavailable flavonoids, thereby negatively

regulating UCP1-driven energy expenditure and promoting exaggerated recurrent weight gain (Fig. 6n). Full validation of this model merits future studies investigating whether the flavonoid effect on BAT *Ucp1* expression directly drives enhanced energy expenditure.

Discussion

In this study, we describe the persistence of an altered microbiome configuration following cycles of obesity and dieting, which contributes to enhanced metabolic derangements upon weight regain, through metabolite-induced effects on host metabolism. We hypothesize that diet-induced microbiome persistence may have evolved to act as a 'buffer' contributing to the stability of metabolic homeostasis over prolonged periods of time, by preventing overly fluctuating metabolic responses to incidental nutritional or environmental signals. However, in contexts of erratic changes in host physiology, such as cycling weight gain and dieting, this microbiome persistence may predispose the host to exaggerated metabolic consequences in ensuing weight-gain cycles. Similar contexts of microbiome persistence include its hysteresis-like behaviour of reduced reversibility during recurrent dietary changes[24], or following low-fibre feeding[25].

Our results highlight two potentially interdependent yet inherently different microbiota effects on weight and metabolism. First, the microbiota from obese donors induces weight gain in faecal transplanted mice even when recipient mice are maintained on a normal chow diet[8,9]. This dominant obesogenic property is lost upon remission of

obesity. Second, the persistent post-dieting microbiota influences the degree of relapsing obesity following weight cycling, but only upon encounter of a 'second hit' that gives rise to recurrent weight gain. While we suggest one mechanism for the common failure of formerly obese individuals to maintain long-term reduced weight after dieting, the reasons for this failure are probably complex and include contributions form a multitude of behavioural, genetic, environmental, and metabolic factors[26]. The findings described here suggest that the remission of metabolic derangements after treatment of obesity precedes the remission of dysbiosis, with the time window of post-obesity microbiome persistence marking the susceptibility phase for accelerated recurrent obesity. Corroboration of these findings in dieting humans as well as additional variables not reflected in mouse models merit further prospective human studies.

Finally, our study provides an example for how rational post-biotic metabolite therapy could serve as a potential means of modulating physiological function downstream of the microbiota. As such, we found that obesity-induced loss of the flavonoids apigenin and naringenin enhances the susceptibility for accelerated weight regain, potentially through impairment of energy expenditure, while replenishment of these metabolites ameliorated these metabolic abnormalities. Future studies are warranted to examine the potential clinical use of flavonoids, as well as modulation of other bioactive metabolites such as bile acids that we found to be persistently elevated after dieting, as novel therapeutics in the quest for effective long-term weight management solutions.

1. Stevens, J., Oakkar, E. E., Cui, Z., Cai, J. & Truesdale, K. P. US adults recommended for weight reduction by 1998 and 2013 obesity guidelines, NHANES 2007-2012. *Obesity (Silver Spring)* **23**, 527–531 (2015).
2. Anastasiou, C. A., Karfopoulou, E. & Yannakoulia, M. Weight regaining: from statistics and behaviors to physiology and metabolism. *Metabolism* **64**, 1395–1407 (2015).
3. Pietiläinen, K. H., Saarni, S. E., Kaprio, J. & Rissanen, A. Does dieting make you fat? A twin study. *Int. J. Obes.* **36**, 456–464 (2012).
4. Neumark-Sztainer, D. *et al.* Obesity, disordered eating, and eating disorders in a longitudinal study of adolescents: how do dieters fare 5 years later? *J. Am. Diet. Assoc.* **106**, 559–568 (2006).
5. Saarni, S. E., Rissanen, A., Sarna, S., Koskenvuo, M. & Kaprio, J. Weight cycling of athletes and subsequent weight gain in middleage. *Int. J. Obes.* **30**, 1639–1644 (2006).
6. Dulloo, A. G. & Montani, J. P. Pathways from dieting to weight regain, to obesity and to the metabolic syndrome: an overview. *Obes. Rev.* **16** (Suppl 1), 1–6 (2015).
7. Mehta, T., Smith, D. L., Jr, Muhammad, J. & Casazza, K. Impact of weight cycling on risk of morbidity and mortality. *Obes. Rev.* **15**, 870–881 (2014).
8. Turnbaugh, P. J. *et al.* An obesity-associated gut microbiome with increased capacity for energy harvest. *Nature* **444**, 1027–1031 (2006).
9. Ridaura, V. K. *et al.* Gut microbiota from twins discordant for obesity modulate metabolism in mice. *Science* **341**, 1241214 (2013).
10. Korem, T. *et al.* Growth dynamics of gut microbiota in health and disease inferred from single metagenomic samples. *Science* **349**, 1101–1106 (2015).
11. David, L. A. *et al.* Diet rapidly and reproducibly alters the human gut microbiome. *Nature* **505**, 559–563 (2014).
12. Liu, J., Lee, J., Salazar Hernandez, M. A., Mazitschek, R. & Ozcan, U. Treatment of obesity with celastrol. *Cell* **161**, 999–1011 (2015).
13. Elinav, E. *et al.* Pegylated leptin antagonist is a potent orexigenic agent: preparation and mechanism of activity. *Endocrinology* **150**, 3083–3091 (2009).
14. Shpilman, M. *et al.* Development and characterization of high affinity leptins and leptin antagonists. *J. Biol. Chem.* **286**, 4429–4442 (2011).
15. Braune, A. & Blaut, M. Bacterial species involved in the conversion of dietary flavonoids in the human gut. *Gut Microbes* **7**, 216–234 (2016).
16. Myoung, H. J., Kim, G. & Nam, K. W. Apigenin isolated from the seeds of *Perilla frutescens* britton var *crispa* (Benth.) inhibits food intake in C57BL/6J mice. *Arch. Pharm. Res.* **33**, 1741–1746 (2010).
17. Guo, X., Liu, J., Cai, S., Wang, O. & Ji, B. Synergistic interactions of apigenin, naringin, quercetin and emodin on inhibition of 3T3-L1 preadipocyte differentiation and pancreas lipase activity. *Obes. Res. Clin. Pract.* **10**, 327–339 (2016).
18. Assini, J. M. *et al.* Naringenin prevents obesity, hepatic steatosis, and glucose intolerance in male mice independent of fibroblast growth factor 21. *Endocrinology* **156**, 2087–2102 (2015).
19. Hoek-van den Hil, E. F. *et al.* Direct comparison of metabolic health effects of the flavonoids quercetin, hesperetin, epicatechin, apigenin and anthocyanins in high-fat-diet-fed mice. *Genes Nutr.* **10**, 469 (2015).
20. Goldwasser, J. *et al.* Transcriptional regulation of human and rat hepatic lipid metabolism by the grapefruit flavonoid naringenin: role of PPARα, PPARγ and LXRα. *PLoS One* **5**, e12399 (2010).
21. Kudo, N. *et al.* A single oral administration of theaflavins increases energy expenditure and the expression of metabolic genes. *PLoS One* **10**, e0137809 (2015).
22. Choi, J. H. & Yun, J. W. Chrysin induces brown fat-like phenotype and enhances lipid metabolism in 3T3-L1 adipocytes. *Nutrition* **32**, 1002–1010 (2016).
23. Suárez-Zamorano, N. *et al.* Microbiota depletion promotes browning of white adipose tissue and reduces obesity. *Nat. Med.* **21**, 1497–1501 (2015).
24. Carmody, R. N. *et al.* Diet dominates host genotype in shaping the murine gut microbiota. *Cell Host Microbe* **17**, 72–84 (2015).
25. Sonnenburg, E. D. *et al.* Diet-induced extinctions in the gut microbiota compound over generations. *Nature* **529**, 212–215 (2016).
26. Montani, J. P., Schutz, Y. & Dulloo, A. G. Dieting and weight cycling as risk factors for cardiometabolic diseases: who is really at risk? *Obes. Rev.* **16** (Suppl 1), 7–18 (2015).

METHODS

Mice. C57Bl/6 mice were purchased from Harlan and allowed to acclimatize to the animal facility environment for 2 weeks before being used for experimentation. In each experiment, all mice were littermates born and raised in the same vivarium and obtained through a single delivery. All mice were maintained on a strict 12-h light–dark cycle (lights turned on at 6 am and turned off at 6 pm) and were housed in cages containing a maximum of five animals. Numbers of animals were chosen to ensure that a minimum of two distinct cages was used per experimental group in each experiment. No statistical methods were used to predetermine sample size. Mice were taken out of experiments when wounded as a result of fighting among cage-mates. Weights were always measured at the same circadian time throughout each experiment. Other than weight and glucose measurements, investigators were blinded with regard to experimental groups. Outbred Swiss Webster germ-free mice were born in the Weizmann Institute germ-free facility and routinely monitored for sterility. For faecal transplantation experiments, 100 mg of stool was resuspended in 1 ml of PBS under anaerobic conditions, homogenized, and filtered through a 70 μm strainer. Recipient mice were gavaged with 200 μl of the filtrate.

All experiments involving weight cycling employed the following experimental paradigm:

1) Before dietary interventions, mice were randomized to ensure that no incidental pre-diet differences in body weight, body fat content, or microbiome composition existed between the different groups (Supplementary Fig. 1).

2) Initial weight gain for 4 weeks ('during obesity' time point, 4 weeks), see also Supplementary Figs 2 and 3.

3) Weight loss until lean control levels are reached (end-point criterion for weight loss: no statistically significant weight difference between cycling group and lean controls; 'after obesity' time point).

4) Weight regain until obese control levels are reached (end-point criterion for weight gain: no statistically significant weight difference between cycling group and obese controls; 'second obesity' time point).

In all experiments, age-matched male mice were used. In Fig. 1h, female mice were used. Mice were 8 weeks of age at the beginning of experiments. For antibiotic treatment, mice were given a combination of vancomycin ($0.5\,\mathrm{g\,l^{-1}}$), ampicillin ($1\,\mathrm{g\,l^{-1}}$), neomycin ($1\,\mathrm{g\,l^{-1}}$), and metronidazole ($1\,\mathrm{g\,l^{-1}}$) in their drinking water[27]. Mice were carefully monitored for signs of dehydration upon antibiotic administration. All antibiotics were obtained from Sigma Aldrich and given for the time periods indicated in each figure. For flavonoid treatments, apigenin and naringenin (obtained from Sigma Aldrich) were dissolved in DMSO and administered daily by oral gavage at a concentration of $80\,\mathrm{mg\,kg^{-1}}$. Controls received vehicle gavages. Celastrol was administered daily by intraperitoneal injection of $100\,\mathrm{\mu g\,kg^{-1}}$ as previously described[12]. Leptin antagonist was administered daily by intraperitoneal injection of $25\,\mathrm{mg\,kg^{-1}}$ as previously described[13].

Rodent diets are detailed in the Supplementary Information (Supplementary Tables 2 and 3). Stool samples were collected fresh and on the basis of individual mice. Fresh stool samples were collected into tubes, immediately snap-frozen in liquid nitrogen upon collection, and stored at $-80\,^\circ\mathrm{C}$ until DNA isolation. All experimental procedures were approved by the local IACUC.

Glucose tolerance test. Mice were fasted for 6 h and subsequently given 200 μl of a $0.2\,\mathrm{g\,ml^{-1}}$ glucose solution (JT Baker) by oral gavage. Blood glucose was determined at 0, 15, 30, 60, 90 and 120 min after glucose challenge (Contour blood glucose meter, Bayer).

Magnetic resonance imaging. Mice were anaesthetized with isofluorane (5% for induction, 1–2% for maintenance) mixed with oxygen ($1\,\mathrm{l\,min^{-1}}$) and delivered through a nasal mask. Once anaesthetized, the animals were placed in a head-holder to assure reproducible positioning inside the magnet. Respiration rate was monitored and kept throughout the experimental period around 60–80 breaths per minute. MRI experiments were performed on 9.4 Tesla BioSpec Magnet 94/20 USR system (Bruker) equipped with gradient coils system capable of producing pulse gradient of up to 40 gauss $\mathrm{cm^{-1}}$ in each of the three directions. All MR images were acquired with a quadrature resonator coil (Bruker). The MRI protocol included two sets of coronal and axial multi-slices T2-weighted MR images. The T2-weighted images were acquired using the multi-slice RARE sequence ($\mathrm{TR} = 2{,}500\,\mathrm{ms}$, $\mathrm{TE} = 35\,\mathrm{ms}$, RARE factor $= 8$), with matrix size being 256×256, four averages, corresponding to an image acquisition time of 160 s per set. The first set was used to acquire 21 axial slices with 1-mm slice thickness (no gap). The field of view was selected with $4.2 \times 4.2\,\mathrm{cm^2}$. The second set was used to acquire 17 coronal slices with 1-mm slice thickness (no gap). The field of view was selected with $7.0 \times 5.0\,\mathrm{cm^2}$. Total fat and lean mass of mice were quantified by EchoMRI-100 (Echo Medical Systems).

Metabolic measurements. Food intake and locomotor activity were measured using the PhenoMaster system (TSE-Systems), which consists of a combination of sensitive feeding sensors for automated measurement and a photobeam-based activity monitoring system detects and records ambulatory movements, including rearing and climbing, in each cage. All parameters were measured continuously and simultaneously. Mice were trained singly housed in identical cages before data acquisition.

Triglycerides, total cholesterol and high-density lipoprotein (HDL) levels were measured in mouse serum by SpotChem EZ Chemistry Analyzer (Arkray). LDL levels were calculated using the Friedewald formula.

Concentrations of leptin (Mouse Leptin DUO set, R&D Systems) and insulin (Ultra-sensitive mouse insulin ELISA kit, Crystal Chem) in the serum were measured using ELISA according to the manufacturer's instructions.

Taxonomic microbiota analysis. Frozen faecal samples were processed for DNA isolation using the MoBio PowerSoil kit according to the manufacturer's instructions. 1 ng of purified faecal DNA was used for PCR amplification. Amplicons spanning the variable region 1/2 (V1/2) of the 16S rRNA gene were generated by using the following barcoded primers: forward, 5′-XXXXXXXXAGAG TTTGATCCTGGCTCAG-3′; reverse, 5′-TGCTGCCTCCCGTAGGAGT-3′, where X represents a barcode base. Amplicons spanning the variable region 3/4 (V3/4) of the 16S rRNA gene (Fig. 2h and Extended Data Fig. 5b–d) were generated by using the following primers: forward, 5′-GTGCCAGCMGCCGCGGTAA-3′; reverse 5′- GGACTACHVGGGTWTCTAAT-3′. The reactions were subsequently pooled and cleaned (PCR clean kit, Promega), and the PCR products were then sequenced on an Illumina MiSeq with 500-bp paired-end reads. The reads were then processed using the QIIME (Quantitative Insights Into Microbial Ecology, http://www.qiime.org) analysis pipeline as described[28–30]. In brief, fasta quality files and a mapping file indicating the barcode sequence corresponding to each sample were used as inputs, reads were split by samples according to the barcode, taxonomical classification was performed using the RDP-classifier, and an OTU table was created. OTU mapping was employed using the Greengenes database. Rarefaction was used to exclude samples with insufficient count of reads per sample. Sequences sharing 97% nucleotide sequence identity in the 16S region were binned into operational taxonomic units (97% ID OTUs). For beta diversity, unweighted UniFrac measurements were plotted according to the two principal coordinates based on >10,000 reads per sample. For microbial distance measurements, unweighted UniFrac distances were compared.

Classification of obesity history. Mouse obesity history was predicted using Random Forest Classification (sklearn 0.15.2) with the features being the relative abundances of 16S OTUs as outputted by QIIME. Classification was made in leave-one-out cross-validation in which each mouse was classified as negative or positive for obesity history.

Prediction of weight regain following HFD diet. Future weight gain of mice was predicted in leave-one-out cross-validation, whereby the weight regain of each mouse upon HFD exposure was predicted using a gradient-boosting regression algorithm using data of all other mice consisting of their 16S rDNA OTU data at the post-dieting nadir period, their obesity history, and their individual weight regain upon HFD exposure. Importantly, each time a mouse was left out and its weight regain was predicted, its obesity history was not given as an input to our algorithm. For each left out mouse, a classifier of obesity history was first learned and used to classify the obesity history of the left out mouse as described above. Then, training data mice with the same obesity history as the left out mouse were taken, and gradient-boosting regression (GBR, sklearn 0.15.2) was applied to learn a model that predicts their weight regain on the HFD diet. Input to this model consists of the 16S OTUs which were used within the GBR algorithm to predict weight regain.

Metagenomic analysis. Metagenomic reads containing Illumina adapters were filtered for exclusion of low-quality reads and trimmed low-quality read edges. Host DNA was detected and excluded by mapping with GEM to the mouse genome with inclusive parameters. Length-normalized RA of genes, obtained by similar mapping with GEM to a reference catalogue[31], was assigned to KEGG Orthology (KO) entries[32], and these were then normalized to a sum of 1. RA of KEGG modules and pathways was calculated by summation. Only samples with >100,000 metagenomics reads were considered for analysis.

Quality control of metagenomic reads and removal of host DNA. We applied Trimmomatic[33] with the following parameters:

ILLUMINACLIP:<Trueseq3 adapters FASTA file>:2:30:10 LEADING:25 TRAILING:25 MINLEN:50. We removed host DNA by mapping to the mouse genome (mm10, downloaded from https://genome.ucsc.edu) and removing any mapped reads (see section below).

Mapping of metagenomic sequencing reads. Mapping was performed using the GEM mapper[34] with the following parameters:

-q offset-33 –gem-quality-threshold 26 -m 0.1 -e 0.1 –min-matched-bases 0.8 –max-big-indel-length 15 -s 3 -d 'all' -D 1 -v -T 2 -p -E 0.3 –max-extendable-matches 'all' –max-extensions-per-match 5

With the addition of the modifier -m set to 0.05 for mapping to the mouse genome. Resulted mappings were retained as long as they had at least 50 matched bases with minimal quality of 26.

Genetic content relative abundance calculation. Reads were mapped to the integrated reference catalogue of the human gut microbiome[31]. For each gene in the catalogue, the fraction of reads mapped to it from each sample was counted and normalized by gene length in kilobases. Reads mapping to more than one location were split so that each location received an equal fraction of the mapped read. Mapped reads were subsequently assigned to KEGG Orthology (KO) entries using the gene annotation table available at http://meta.genomics.cn/. Relative gene abundances were then calculated by normalizing the KEGG genes of each sample to sum to 1. To calculate the abundances of KEGG pathways and modules, the relative abundance of genes in each pathway and module was summed.

Non-targeted metabolomics. Caecal samples were collected, immediately frozen in liquid nitrogen and stored at $-80\,°C$. Sample preparation and analysis was performed by Metabolon Inc. Samples were prepared using the automated MicroLab STAR system (Hamilton). To remove protein, dissociate small molecules bound to protein or trapped in the precipitated protein matrix, and to recover chemically diverse metabolites, proteins were precipitated with methanol. The resulting extract was divided into five fractions: one for analysis by UPLC-MS/MS with positive ion mode electrospray ionization, one for analysis by UPLC-MS/MS with negative ion mode electrospray ionization, one for LC polar platform, one for analysis by GC-MS, and one sample was reserved for backup. Samples were placed briefly on a TurboVap (Zymark) to remove the organic solvent. For LC, the samples were stored overnight under nitrogen before preparation for analysis. For GC, each sample was dried under vacuum overnight before preparation for analysis.

Data extraction and compound identification. Raw data was extracted, peak-identified and QC processed using Metabolon's hardware and software. Compounds were identified by comparison to library entries of purified standards or recurrent unknown entities.

Metabolite quantification and data normalization. Peaks were quantified using area-under-the-curve. For studies spanning multiple days, a data normalization step was performed to correct variation resulting from instrument inter-day tuning differences.

Flavonoid measurements. Apigenin and naringenin were measured by Waters TQ MS detector combined with Waters Acquity UPLC system. The chromatographic separation was carried out on a BEH C18 column ($1.7\,\mu m$, $2.1 \times 100\,mm$, Waters). The solvent flow rate was $0.3\,ml\,min^{-1}$. The mobile phase consisted of 0.1% formic acid (FA) in 5% acetonitrile (A) and 0.1% FA in acetonitrile (B) using a gradient program described below. The autosampler was cooled to $12\,°C$ and the column heated to $35\,°C$. MS detector (Waters TQ) was equipped with an ESI source used in positive mode (capillary voltage 2.5 kV). The measurement was performed in MRM mode, two MRM traces for each compound (one for quantification, and the second for identification). The cone voltages (V) and collision energies (eV) for each MRM transition, as determined by direct injection, are summarized below. Data were processed with MassLynx software with TargetLynx (version 4.1, Waters).

For sample preparation, 50 mg of stool or 100 mg food were weighed into 2-ml safe-lock Eppendorf tubes. Samples were homogenized using a beadbeater with metal balls. Three-hundred micrograms of 80% methanol in DDW were added to the samples, followed by sonication for 20 min, centrifugation, and filtering through Acrodisc PTFE 0.2 μm filters (P/N 4552T) into vials.

See Supplementary Table 4 for chromatographic conditions for flavonoid separation.

Gene expression analysis. Tissues were preserved in RNAlater solution (Ambion) and subsequently homogenized in Tri Reagent (Sigma Aldrich). RNA was purified using standard chloroform extraction. Two micrograms of total RNA was used to generate cDNA (HighCapacity cDNA Reverse Transcription kit; Applied Biosystems). Real-time PCR was performed using the following *Ucp1* primers: *Ucp1* forward, 5′-GGCCTCTACGACTCAGTCCA-3′; *Ucp1* reverse, 5′-TAA GCCGGCTGAGATCTTGT-3′. Primers for flavanone 4-reductase and chalcone were tested using http://insilico.ehu.eus/PCR/ and validated using cultures of *Lactococcus lactis* and *Escherichia coli*.

PCR was performed using Kapa Sybr qPCR kit (Kapa Biosystems) on a Viia7 instrument (Applied Biosystems). PCR conditions were $95\,°C$ for $20\,s$, followed by 40 cycles of $95\,°C$ for $3\,s$ and $60\,°C$ for $30\,s$. Data were analysed using the $\Delta\Delta^{C_t}$ method with *Hprt* serving as the reference housekeeping gene. *Hprt* cycles were assured to be insensitive to the experimental conditions.

Western blot analysis. Brown adipose tissue samples were excised and washed thoroughly with PBS, homogenized in RIPA buffer containing protease inhibitors, incubated for 20 min in $4\,°C$ and centrifuged for 20 min, 14,000 r.p.m., at $4\,°C$. Samples were separated on 12% acrylamide gels and transferred onto nitrocellulose membranes. Western blot analysis was performed using anti-UCP1 (M-17) polyclonal antibody (Santa Cruz, sc-6529) and donkey anti-goat antibody (Jackson ImmunoResearch, 705-035-003). Band density was calculated using ImageJ software. See Supplementary Fig. 4 for immunoblot source data.

Adipose tissue explants. Brown adipose tissue was excised and rinsed with PBS. The tissue explants were cultured with 0, 10 or 100 μM of apigenin and naringenin for 24 h in DMEM medium containing 10% FBS, L-glutamine, penicillin, and streptomycin at $37\,°C$. Explants were then collected and immediately processed for qPCR and western blot analysis as described above.

Statistical analysis. Data are expressed as mean ± s.e.m. Comparisons between two groups were performed using two-tailed Mann–Whitney *U*-test. ANOVA was used for comparison between multiple groups. Statistical testing was performed using GraphPad Prism software. *K*-means clustering based on Pearson's correlation was used to classify the temporal behaviour of OTUs, metagenomes, and metabolites in weight-cycling mice after normalization to control mice in order to account for ageing-induced changes. P values <0.05 were considered significant. *$P < 0.05$; **$P < 0.01$; ***$P < 0.001$; ****$P < 0.0001$. Exact P values for each experiment can be found in Supplementary Table 6.

Data availability. The sequencing data has been deposited at the European Nucleotide Archive database with the accession number PRJEB17697 and are available from the corresponding authors upon request.

27. Rakoff-Nahoum, S., Paglino, J., Eslami-Varzaneh, F., Edberg, S. & Medzhitov, R. Recognition of commensal microflora by toll-like receptors is required for intestinal homeostasis. *Cell* **118**, 229–241 (2004).
28. Caporaso, J. G. *et al.* QIIME allows analysis of high-throughput community sequencing data. *Nat. Methods* **7**, 335–336 (2010).
29. Thaiss, C. A. *et al.* Transkingdom control of microbiota diurnal oscillations promotes metabolic homeostasis. *Cell* **159**, 514–529 (2014).
30. Levy, M. *et al.* Microbiota-modulated metabolites shape the intestinal microenvironment by regulating NLRP6 inflammasome signaling. *Cell* **163**, 1428–1443 (2015).
31. Li, J. *et al.* An integrated catalog of reference genes in the human gut microbiome. *Nat. Biotechnol.* **32**, 834–841 (2014).
32. Kanehisa, M. & Goto, S. KEGG: Kyoto encyclopedia of genes and genomes. *Nucleic Acids Res.* **28**, 27–30 (2000).
33. Bolger, A. M., Lohse, M. & Usadel, B. Trimmomatic: a flexible trimmer for Illumina sequence data. *Bioinformatics* **30**, 2114–2120 (2014).
34. Marco-Sola, S., Sammeth, M., Guigó, R. & Ribeca, P. The GEM mapper: fast, accurate and versatile alignment by filtration. *Nat. Methods* **9**, 1185–1188 (2012).
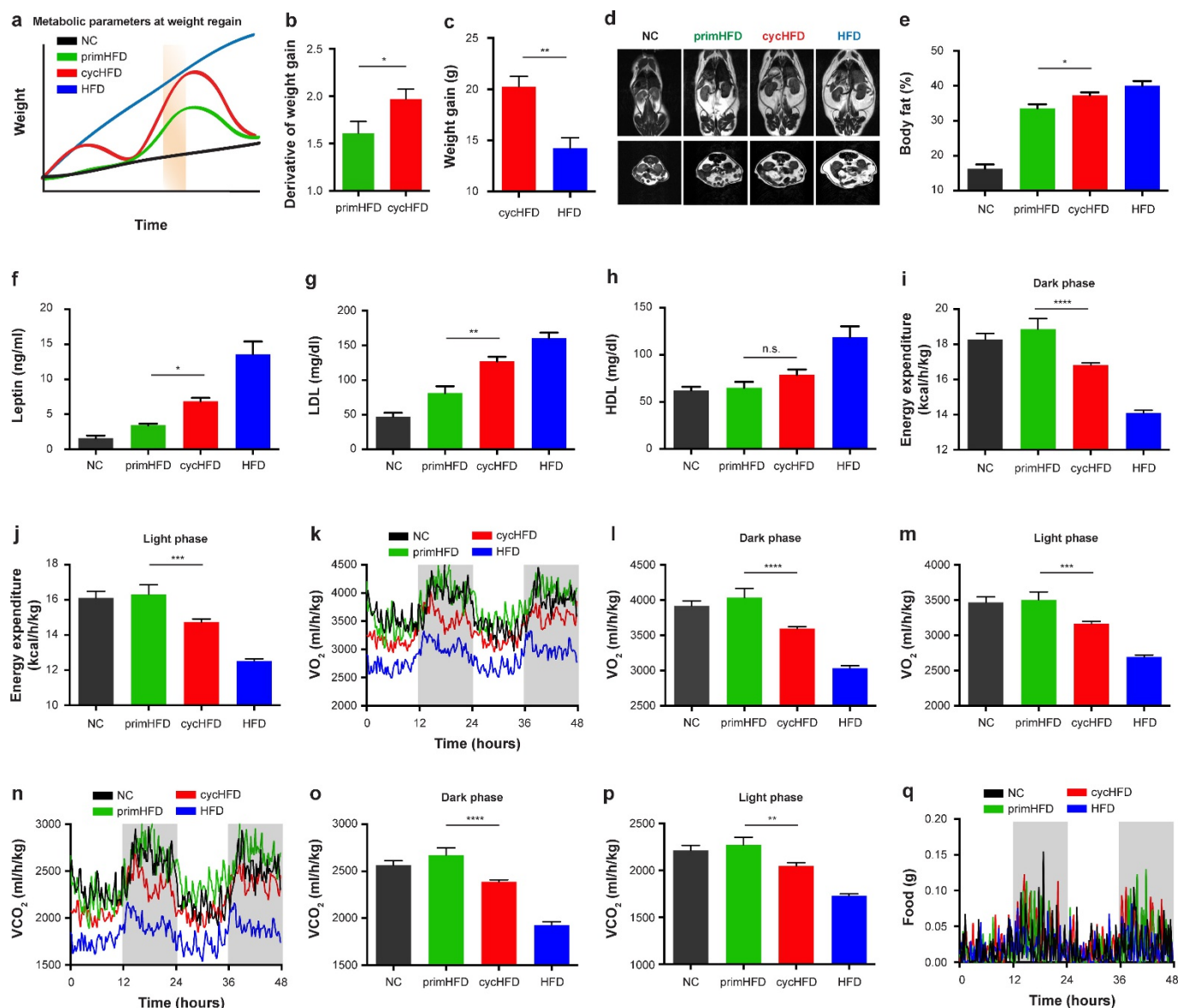
Extended Data Figure 1 | Metabolic measurements during weight regain. a, Schematic indicating time point of metabolic measurements. **b**, Quantification of weight regain by weight gain. **c**, Net weight gain induced by 8 weeks of HFD in weight-cycling mice and continuous HFD. **d**, **e**, Coronal (above) and axial (below) MRI scans (**d**), and quantification of body fat content (**e**). **f**–**h**, Serum levels of leptin (**f**), LDL (**g**), and HDL (**h**) during the second HFD exposure of mice undergoing weight cycling and controls. **i**, **j**, Quantification of dark phase (**i**) and light phase (**j**) energy expenditure upon weight regain of weight-cycling mice. **k**–**q**, Representative recordings (**k**, **n**, **q**) and quantifications (**l**, **m**, **o**, **p**) of O_2 consumption (**k**–**m**), CO_2 consumption (**n**–**p**), and food intake (**q**) upon weight regain of weight-cycling mice. Experiments were repeated twice. Shown are mean ± s.e.m. *$P < 0.05$; **$P < 0.01$; ***$P < 0.001$; ****$P < 0.0001$ by ANOVA (**e**–**p**) or Mann–Whitney U-test (**b**, **c**). See Supplementary Tables 5 and 6 for exact n and P values.
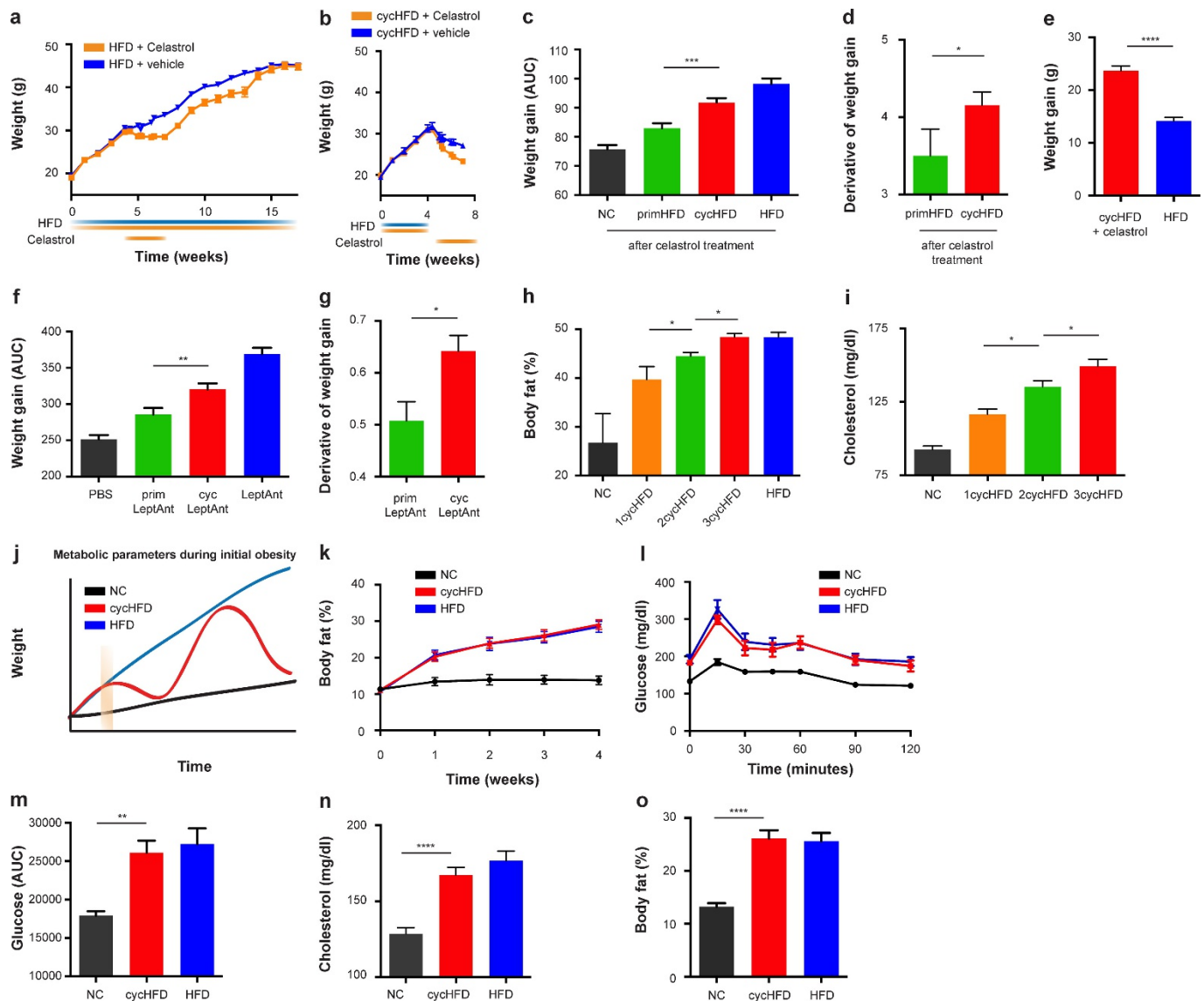
Extended Data Figure 2 | Enhanced recurrent weight gain after initial obesity. a, b, The effect of celastrol on weight loss in mice continuously fed a HFD (**a**) and mice with alternating diets (**b**). **c–e**, Weight regain quantification by AUC (**c**), weight regain slope (**d**), and net weight gain on HFD (**e**) by control mice and weight-cycling mice treated with celastrol to lose weight. **f, g**, Quantification of weight regain by AUC (**f**), weight regain slope (**g**) of leptin antagonist-treated weight-cycling mice and controls. **h, i**, Body fat content (**h**), and serum cholesterol levels (**i**) of weight-cycling mice undergoing a third weight cycle and controls. **j**, Schematic of the analysed time point in **k–o**. **k**, Weight gain during 4 weeks of HFD. **l–o**, Glucose levels after glucose tolerance test (**l**), glucose level quantification (**m**), serum cholesterol levels (**n**), and quantification of body fat content (**o**) in weight-cycling mice during initial obesity and controls. Experiments were repeated twice. Shown are mean ± s.e.m. *$P < 0.05$; **$P < 0.01$; ***$P < 0.001$; ****$P < 0.0001$ by ANOVA (**c, f, h, i, m, n, o**) or Mann–Whitney U-test (**d, e, g**). See Supplementary Tables 5 and 6 for exact n and P values.
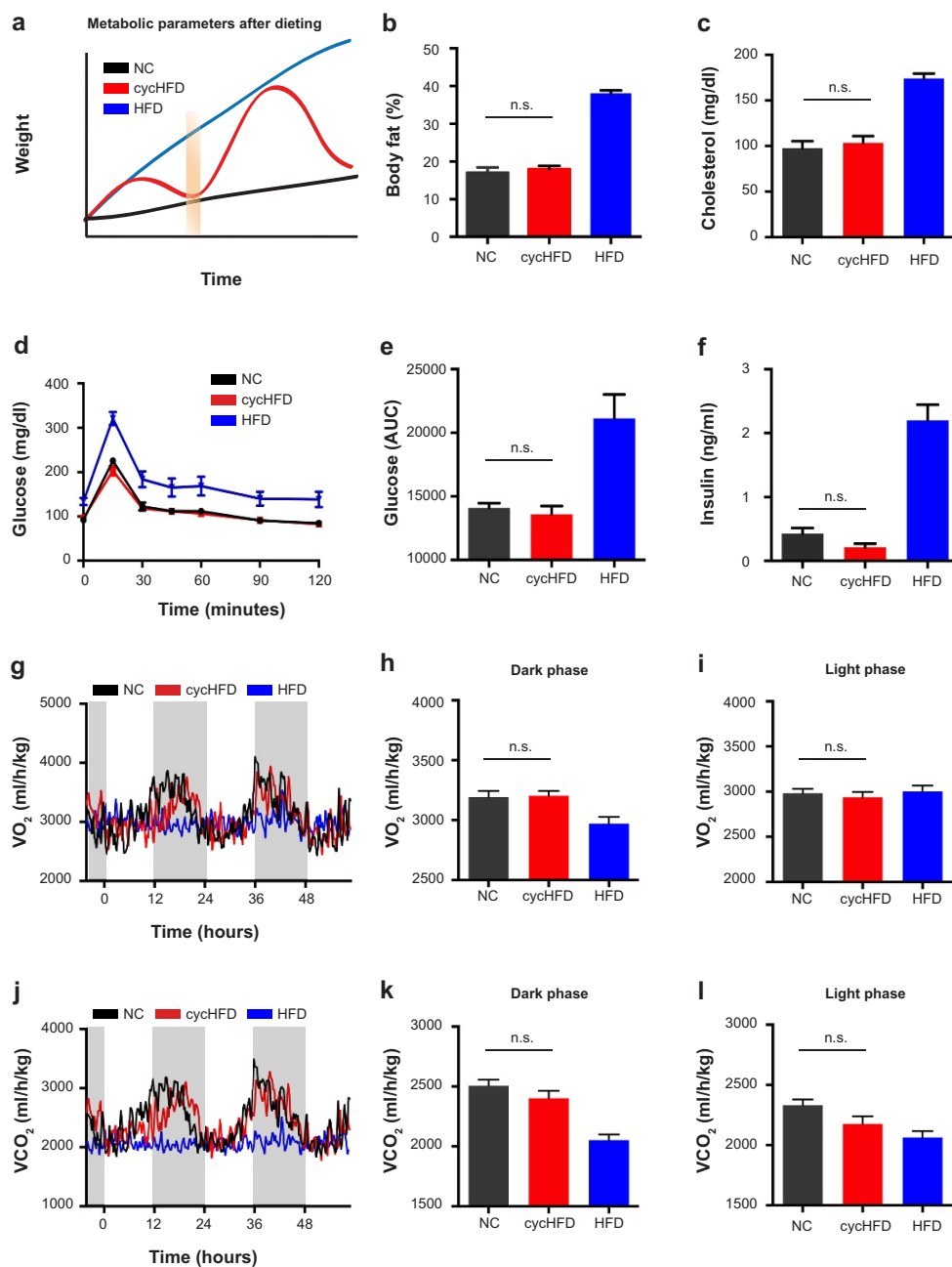
Extended Data Figure 3 | Recovery of metabolic parameters after dieting. a, Schematic of the analysed nadir time point. **b–f**, Body fat content (**b**), serum cholesterol levels (**c**), glucose levels after glucose tolerance test (**d**), glucose level quantification (**e**), and serum insulin levels (**f**) in weight-cycling mice upon return to normal weight.

g–l, Representative recordings (**g, j**) and quantifications (**h, i, k, l**) of O_2 and CO_2 consumption by weight-cycling mice upon return to normal weight and controls. Experiments were repeated twice. Data are mean ± s.e.m. n.s., not significant by ANOVA. See Supplementary Table 5 for exact *n* values.
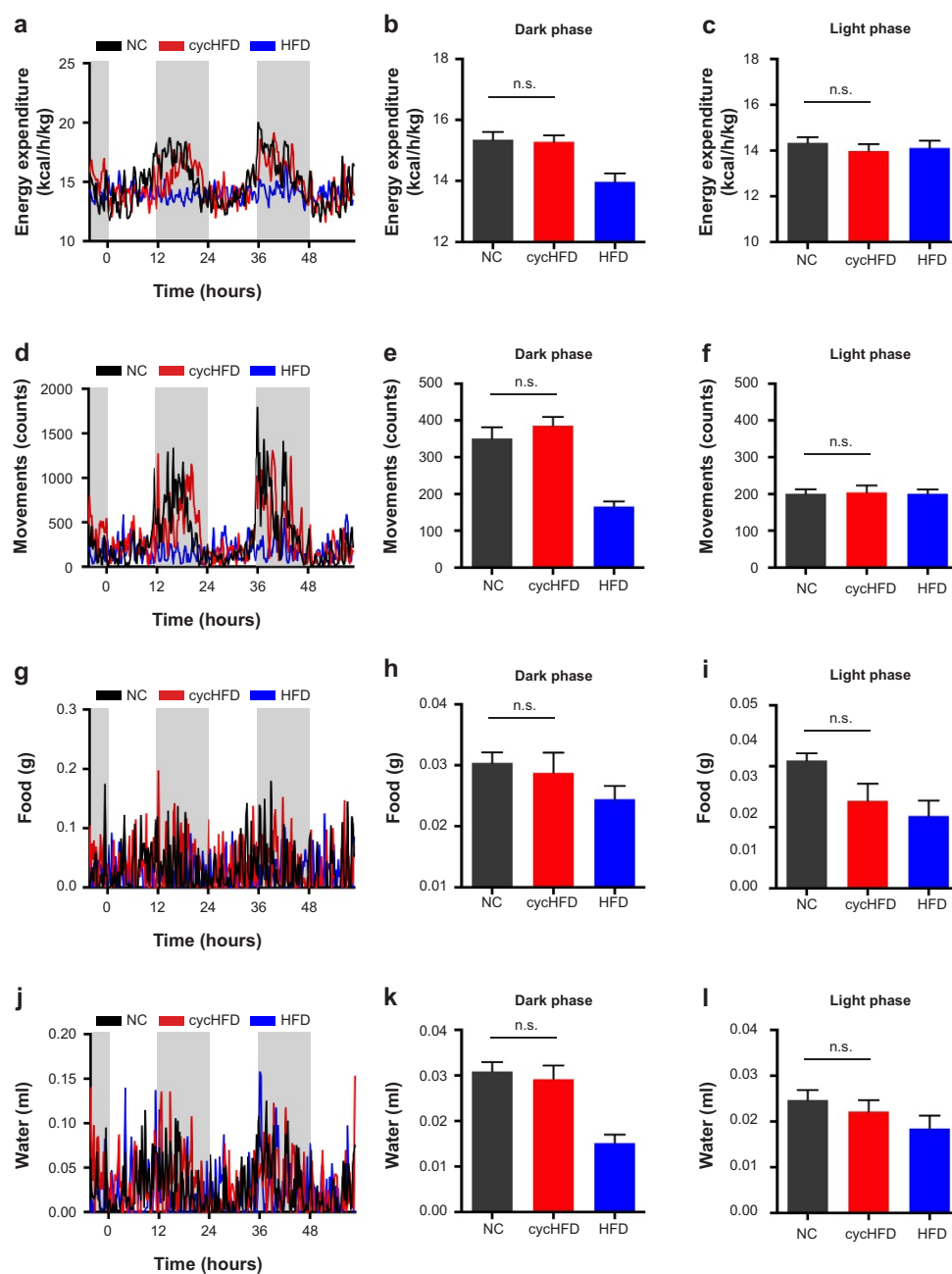
Extended Data Figure 4 | Metabolic measurements after dieting.
Representative recordings (**a**, **d**, **g**, **j**), dark phase (**b**, **e**, **h**, **k**), and light phase (**c**, **f**, **i**, **l**) quantifications of energy expenditure (**a–c**), physical activity (**d–f**), food intake (**g–i**), and water consumption (**j–l**) of weight-cycling mice during weight regain and controls. Experiments were repeated twice. Shown are mean ± s.e.m. n.s., not significant by ANOVA. See Supplementary Table 5 for exact *n* values.
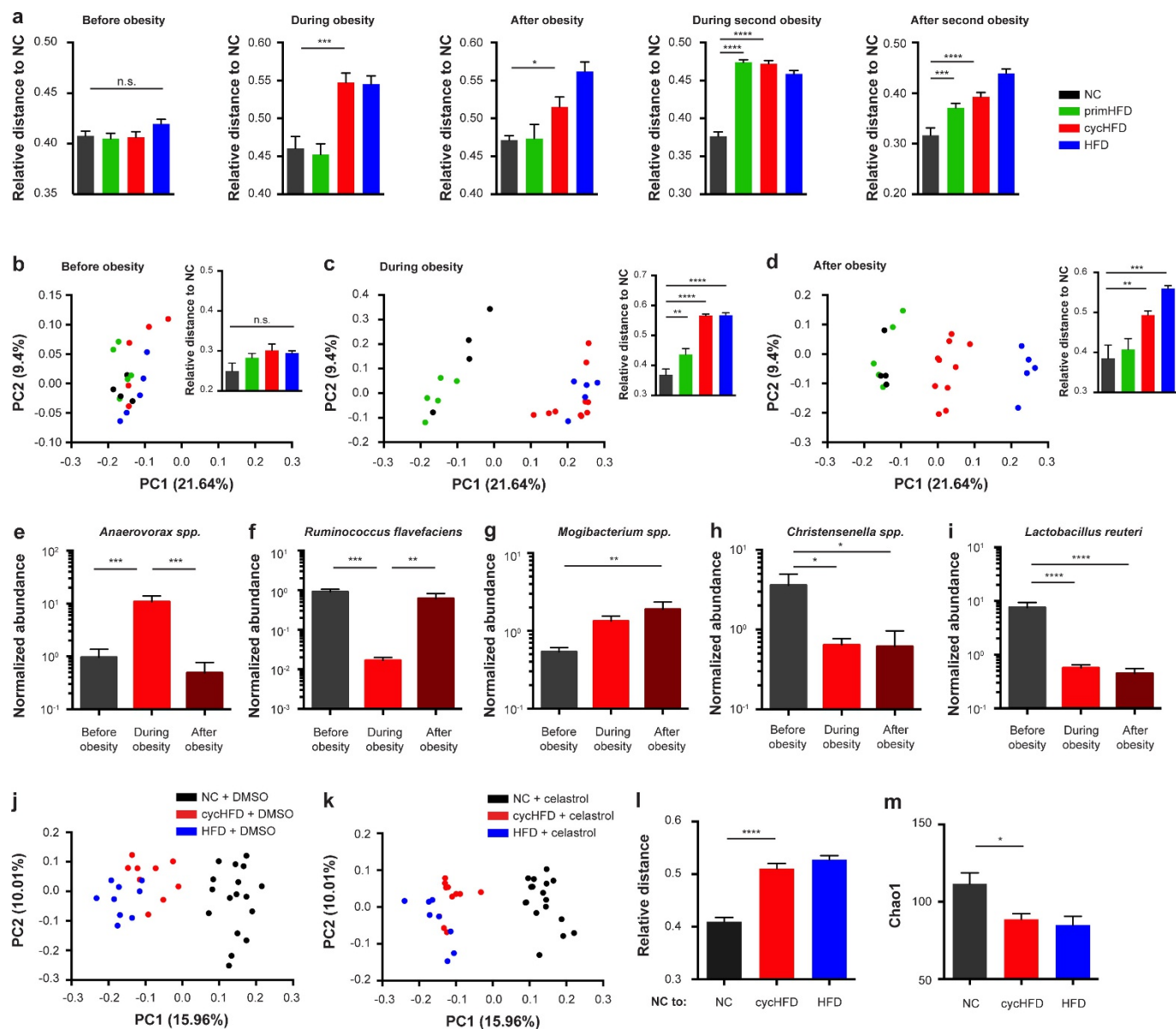
**Extended Data Figure 5 | Persistent microbiome changes after dieting.**
a, Quantification of UniFrac distances of weight-cycling mice from NC controls at the indicated time points. Plots correspond to the PCoA analyses in Fig. 2b–f. **b–d**, PCoA analyses and distance quantification (insets) of V3/V4-targeted 16S sequencing of mice before (**b**), during (**c**), and after (**d**) diet-induced obesity and subsequent weight loss. **e–i**, Examples of OTUs whose abundance does (**e, f**) or does not (**g–i**)

recover after dieting. **j–m**, PCoA analyses (**j, k**), UniFrac distance (**l**) and alpha diversity (**m**) at the nadir time point of post-dieting mice that had received celastrol to accelerate weight loss. Experiments were repeated twice. Data are mean ± s.e.m. *$P < 0.05$, **$P < 0.01$, ***$P < 0.001$, ****$P < 0.0001$ by ANOVA. See Supplementary Tables 5 and 6 for exact n and P values.
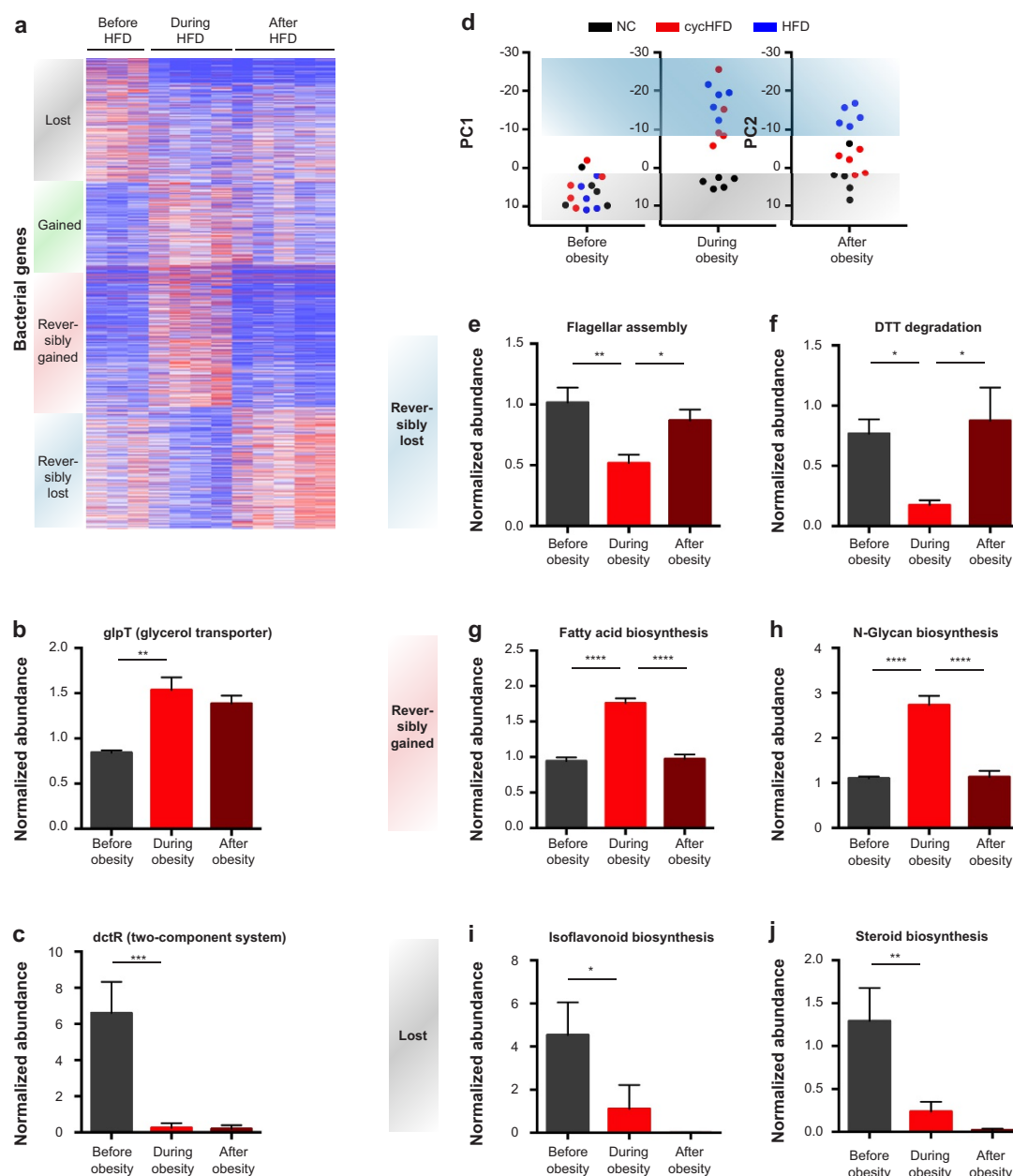
Extended Data Figure 6 | Persistent metagenomic changes after dieting. a, Heatmap of normalized gene abundance in the microbiota of mice before, during, and after obesity. **b**, **c**, Examples of genes whose abundance does not recover after dieting. **d**, PCA of bacterial KEGG modules over time in weight-cycling mice and controls. **e**–**j**, Examples of KEGG pathways whose abundance is reversibly decreased (**e**, **f**), reversibly increased (**g**, **h**), or persistently decreased (**i**, **j**) during obesity and dieting. Data are from one experiment. Data are mean ± s.e.m. *$P < 0.05$, **$P < 0.01$, ***$P < 0.001$, ****$P < 0.0001$ by ANOVA. See Supplementary Tables 5 and 6 for exact n and P values.
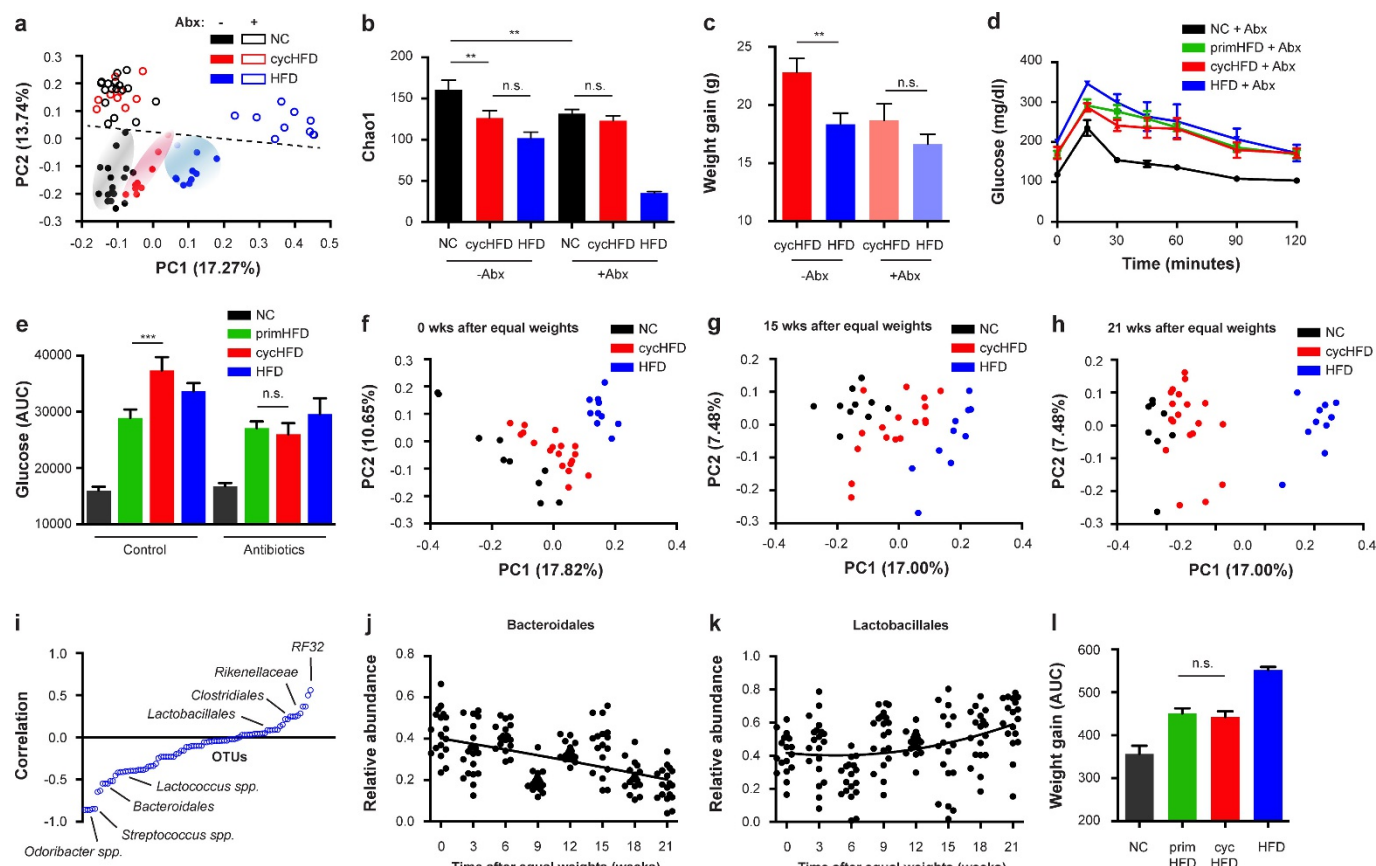
Extended Data Figure 7 | The post-dieting microbiota drives enhanced recurrent obesity. a, **b**, PCoA (**a**) and alpha diversity (**b**) of faecal microbiota after dieting (nadir time point at week 8) from mice with or without antibiotic treatment during weight loss. **c**, Net weight gain induced by 8 weeks of HFD in weight-cycling mice or continuous HFD control with or without antibiotic treatment between weeks 4 and 8. **d**, **e**, Glucose levels after oral glucose tolerance test (**d**) and glucose level quantification after glucose tolerance test (**e**) during weight regain in mice with or without antibiotic treatment during weight loss ($n = 4–10$).

f–h, PCoA of faecal microbiota from formerly obese mice and controls at the time of dieting-induced weight normalization (**f**), 15 weeks after weight normalization (**g**), and 21 weeks after weight normalization (**h**). **i–k**, Correlation analysis (**i**) and examples (**j**, **k**) of microbial taxa undergoing gradual normalization in abundance over a period of 21 weeks after weight normalization. **l**, Quantification of secondary weight gain after microbiota normalization. Experiments were repeated twice. Data are mean ± s.e.m. **$P < 0.01$, ***$P < 0.001$ by ANOVA. See Supplementary Tables 5 and 6 for exact n and P values.
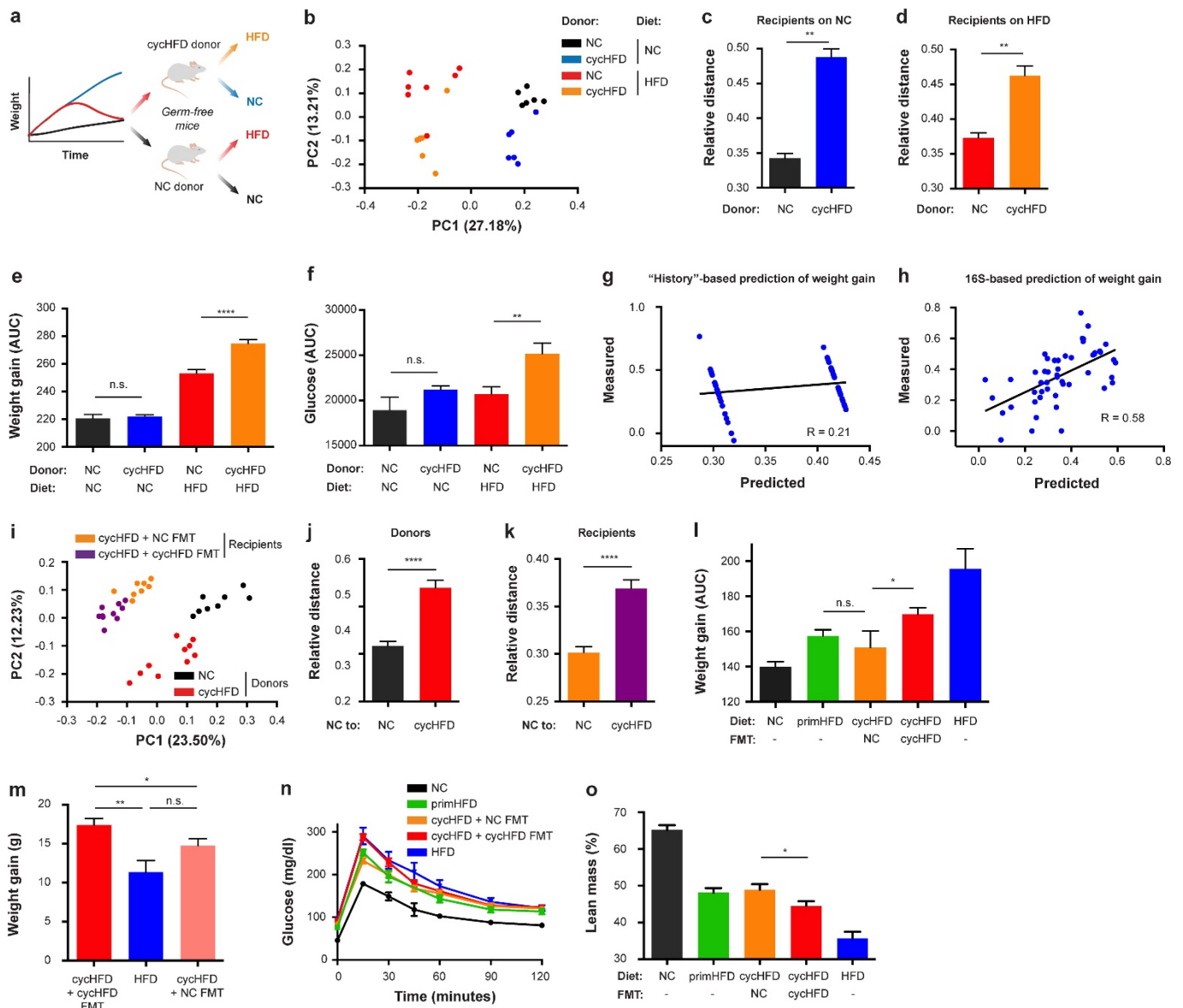
Extended Data Figure 8 | Transfer, prediction and treatment of weight regain by microbiome features. a, Schematic of microbiota transfer to germ-free mice after dieting. Recipients were fed either a HFD or NC. **b–d**, PCoA of recipient microbiota (**b**) and relative UniFrac distances to NC controls (**c**, **d**) of germ-free mice one week after transplantation with microbiota from weight-cycling mice or controls, and fed either NC (**c**) or a HFD (**d**). **e**, **f**, Quantifications of weight gain (**e**) and blood glucose after glucose tolerance test (**f**) in germ-free recipients of microbiota from weight cycling mice or controls. **g**, **h**, Correlation of predicted and measured weight gain when prediction is based solely on inferred history of

obesity (**g**) or solely on 16S sequencing (**h**). **i–k**, PCoA of faecal microbiota (**i**) and relative UniFrac distances between donors (**j**) and recipients (**k**) two weeks after the onset of daily FMT from cycHFD or NC mice to mice undergoing weight cycling. **l–o**, Quantification of secondary weight gain (**l**), net weight gain induced by 8 weeks of HFD feeding (**m**), glucose levels after glucose tolerance test (**n**) and lean mass (**o**) in weight-cycling mice and controls with or without FMT. Experiments were repeated twice. Data are mean ± s.e.m. n.s., not significant. *$P < 0.05$, **$P < 0.01$, ****$P < 0.0001$ by ANOVA (**e**, **f**, **l**, **m**, **o**) or Mann–Whitney U-test (**c**, **d**, **j**, **k**). See Supplementary Tables 5 and 6 for exact n and P values.
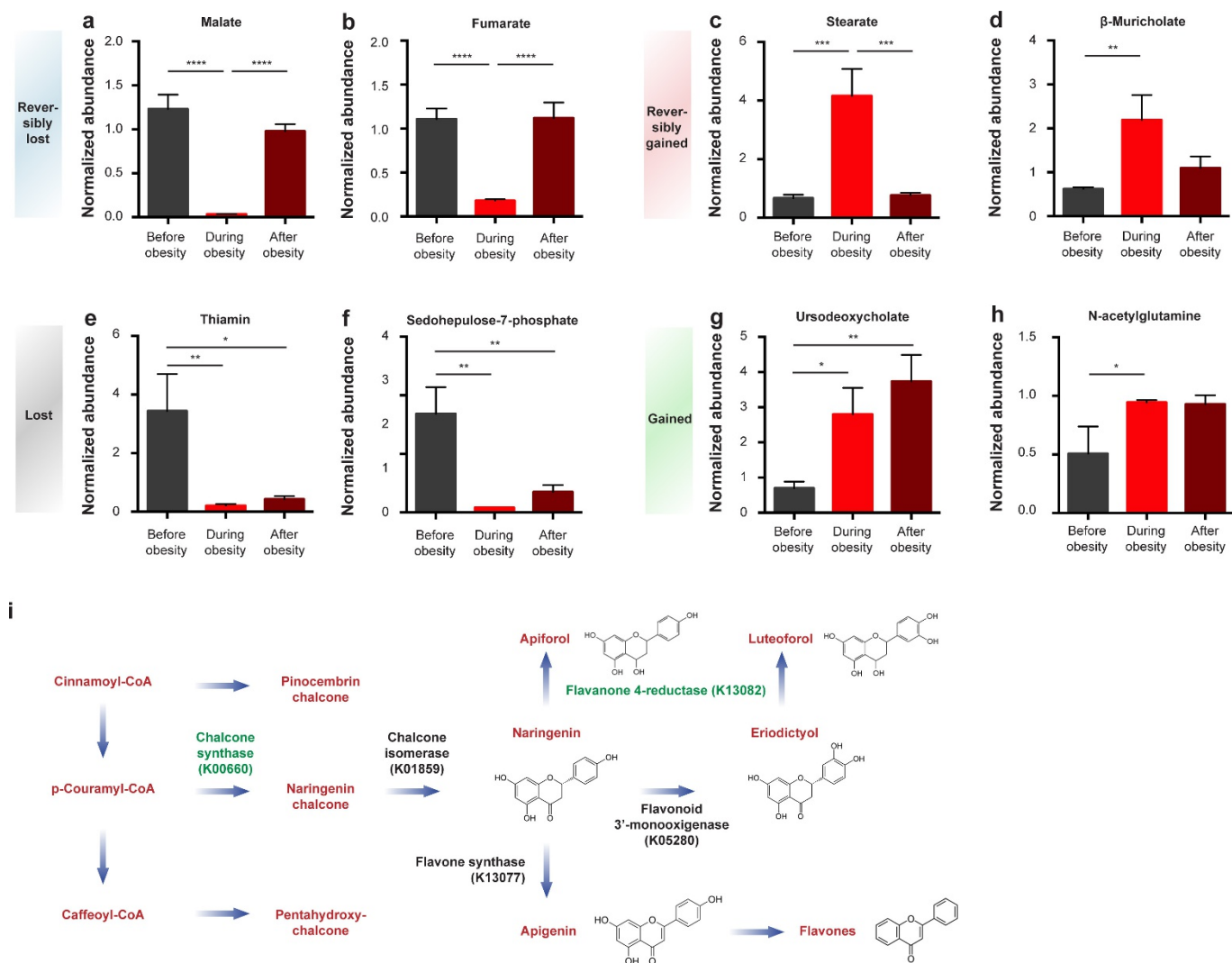
**Extended Data Figure 9 | Persistent metabolomic changes after dieting. a–h**, Examples of metabolites whose abundance is reversibly decreased (**a, b**), reversibly increased (**c, d**), persistently decreased (**e, f**), or persistently increased (**g, h**) during obesity and dieting. **i**, Schematic of flavonoid biosynthetic pathways leading to the production and conversion of naringenin. KEGG IDs of key enzymes are indicated. Genes found in our metagenomic dataset are indicated in green. Data are from one experiment. Shown are mean ± s.e.m. *$P < 0.05$, **$P < 0.01$, ***$P < 0.001$, ****$P < 0.0001$ by ANOVA. See Supplementary Tables 5 and 6 for exact n and P values.
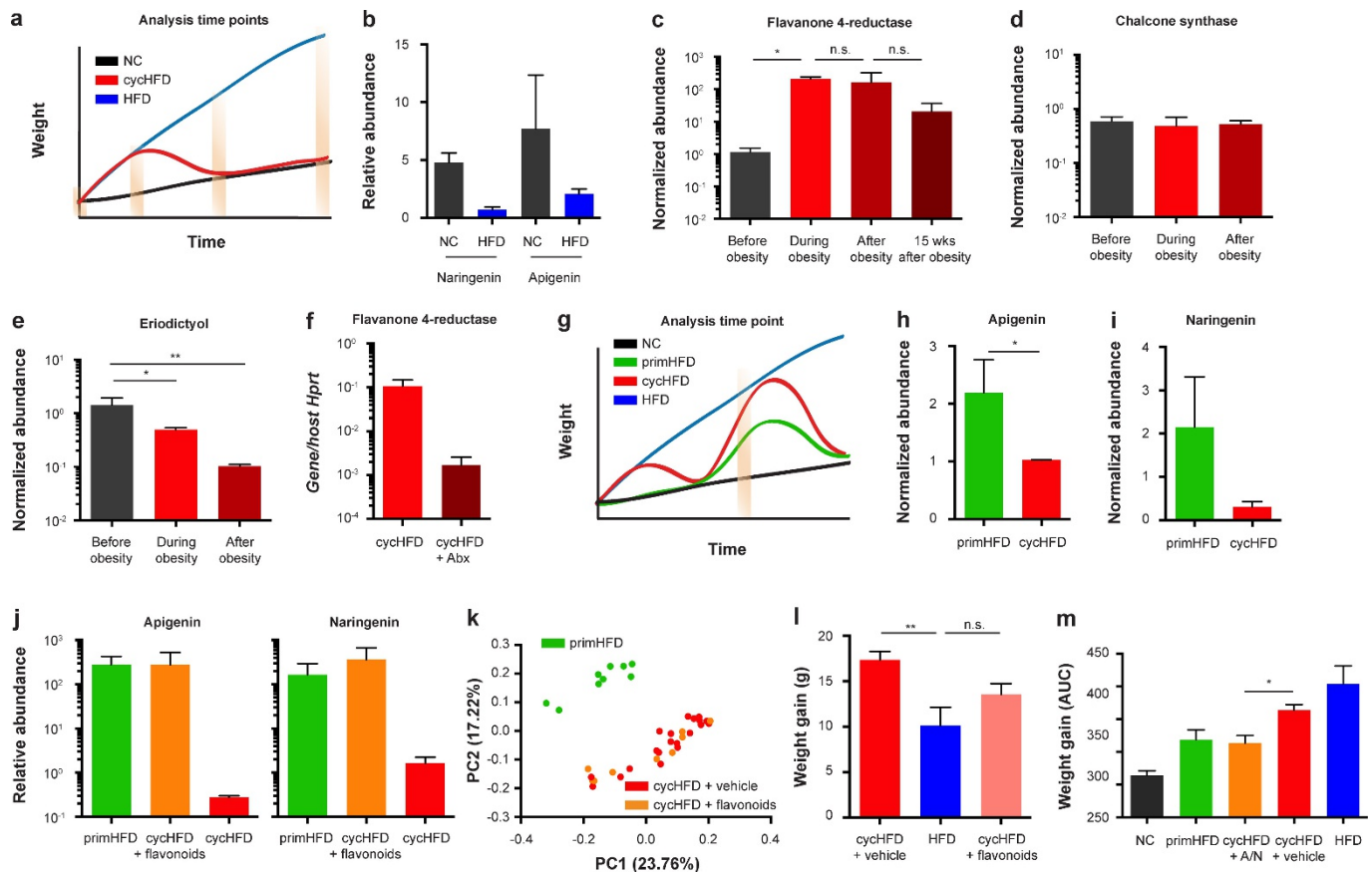
Extended Data Figure 10 | Microbiota control of post-dieting metabolic complications through intestinal flavonoids. a, Schematic showing sampling times in obesity/recovery cycle experiment. **b**, Dietary flavonoids in NC and HFD. **c–e**, Abundance of flavanone 4-reductase (**c**), chalcone synthase (**d**), and eriodictyol (**e**) over time in the faeces of mice undergoing weight cycling normalized to controls. **f**, Quantification of flavanone 4-reductase levels in faecal DNA relative to host DNA in weight-cycling mice at the end of the weight loss period, with or without antibiotic treatment during weight loss. **g**, Schematic of sampling time upon weight regain. **h, i**, Abundance of apigenin (**h**) and naringenin (**i**) in the faeces of mice undergoing post-dieting weight regain and controls. **j–m**, Flavonoid levels (**j**), PCoA of faecal microbiota (**k**), net weight gain induced by 8 weeks of HFD (**l**), and weight regain quantification by AUC (**m**) of weight-cycling mice supplemented with apigenin and naringenin during the weight regain. Data are from one (**a–k**) or two (**l, m**) experiments. Shown are mean ± s.e.m. *$P < 0.05$, **$P < 0.01$ by ANOVA (**c, e, l**) or Mann–Whitney U-test (**h, m**). See Supplementary Tables 5 and 6 for exact n and P values.
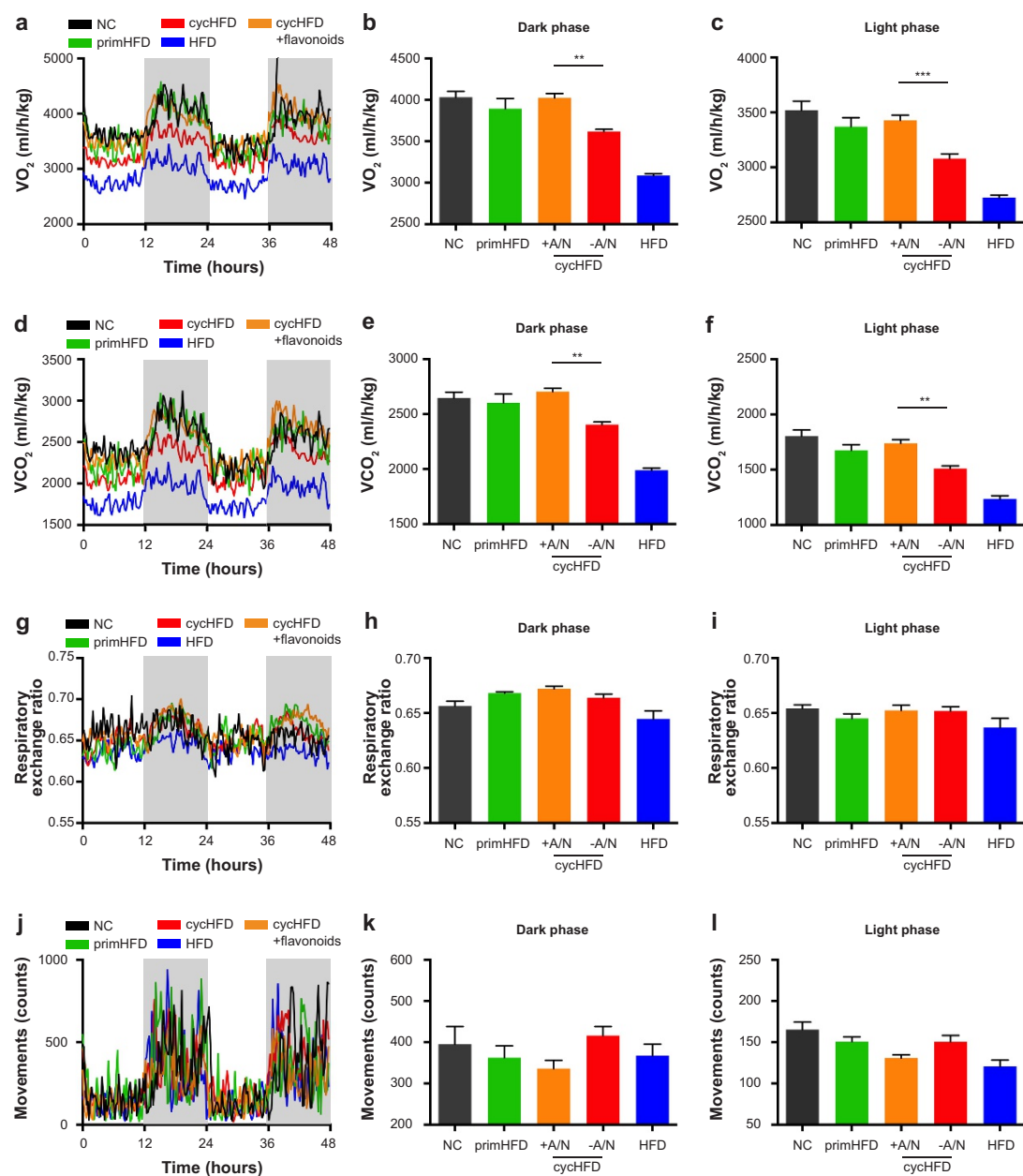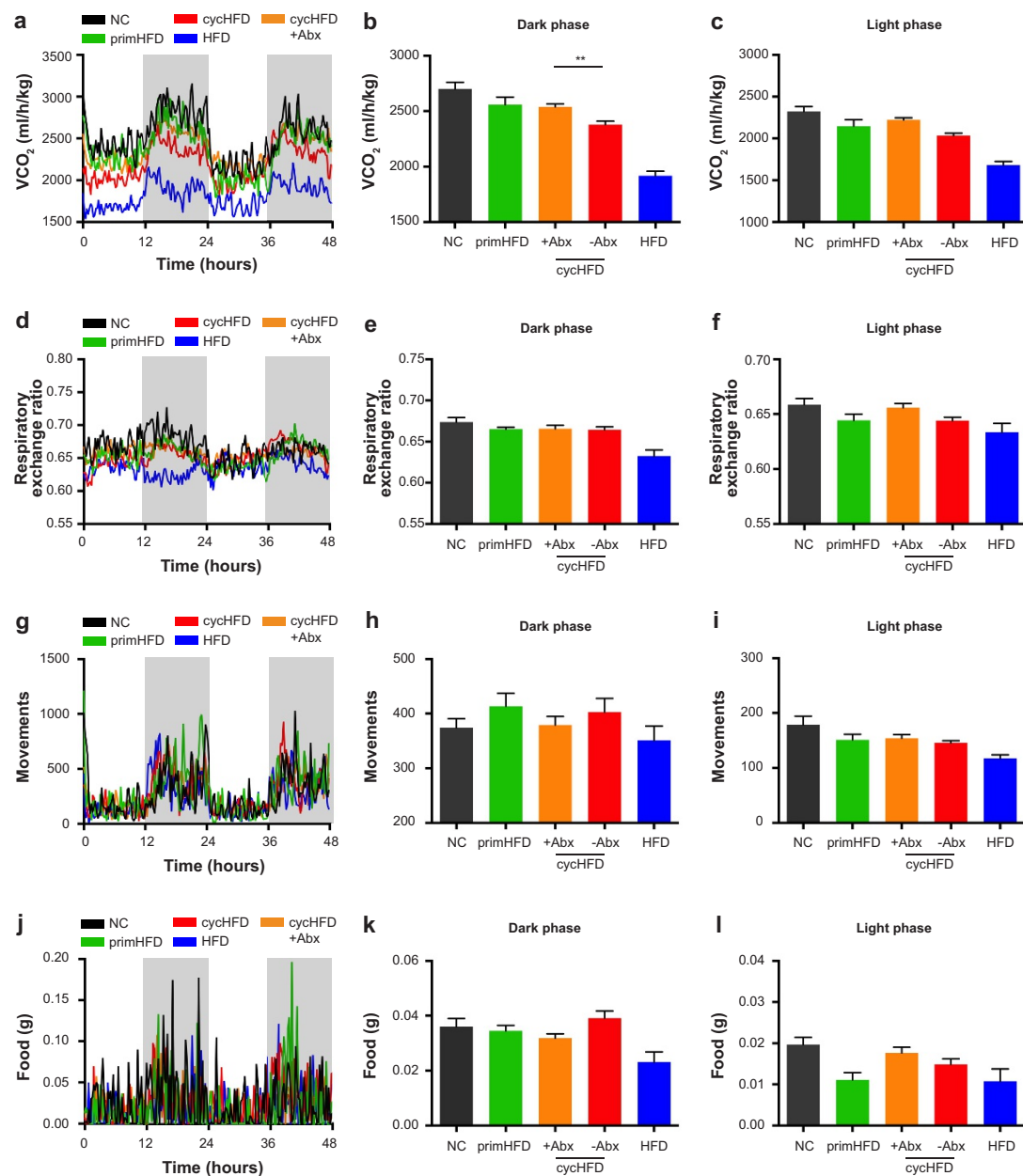
Extended Data Figure 11 | Metabolic measurements in flavonoid-treated mice. Representative recordings (**a**, **d**, **g**, **j**), dark phase quantifications (**b**, **e**, **h**, **k**), and light phase quantifications (**c**, **f**, **i**, **l**) of O_2 consumption (**a–c**), CO_2 consumption (**d–f**), respiratory exchange ratio (**g–i**), and physical activity (**j–l**) of weight-cycling mice with or without supplementation of apigenin and naringenin (A/N) during weight regain. Data are from one experiment. Data are mean ± s.e.m. **$P < 0.01$, ***$P < 0.001$ by ANOVA. See Supplementary Tables 5 and 6 for exact n and P values.
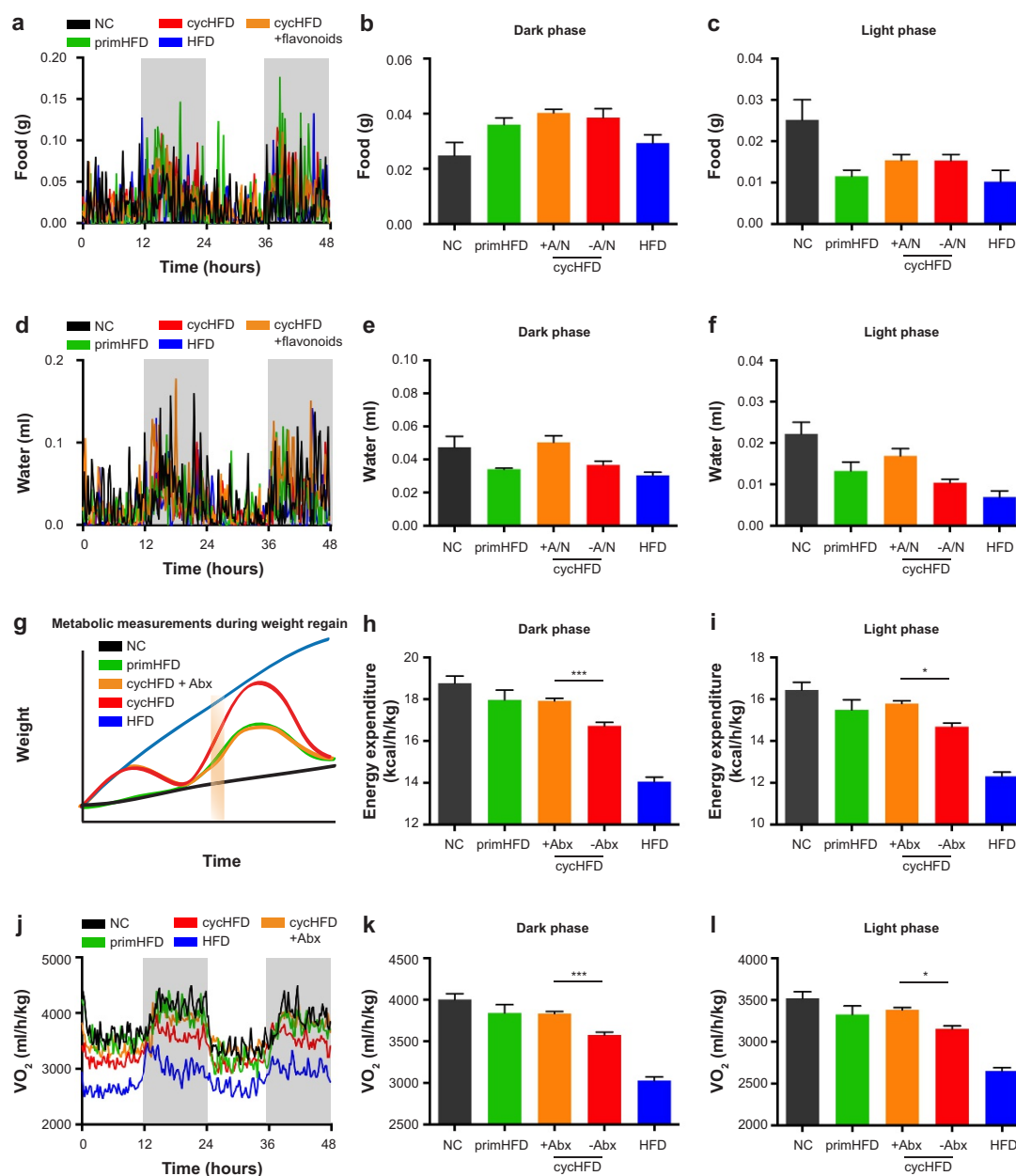
Extended Data Figure 12 | Metabolic measurements in flavonoid- and antibiotic-treated mice. Representative recordings (**a**, **d**), dark phase quantifications (**b**, **e**), and light phase quantifications (**c**, **f**) of food (**a**–**c**) and water consumption (**d**–**f**), of weight-cycling mice with or without supplementation of apigenin and naringenin (A/N) during weight regain. **g**, Schematic indicating time of metabolic measurements during the weight regain phase. **h**, **i**, Quantifications of energy expenditure in weight-cycling mice with or without antibiotic treatment during weight loss. **j**–**l**, Representative recording (**j**) and quantifications (**k**, **l**) of O_2 consumption by weight-cycling mice with or without antibiotic treatment (Abx) during weight loss. Data are from one experiment. Shown are mean ± s.e.m. *$P < 0.05$, ***$P < 0.001$ by ANOVA. See Supplementary Tables 5 and 6 for exact n and P values.

Extended Data Figure 13 | Metabolic measurements in antibiotic-treated mice. Representative recordings (**a**, **d**, **g**, **f**), dark phase quantifications (**b**, **e**, **h**, **k**), and light phase quantifications (**c**, **f**, **i**, **l**) of CO_2 consumption (**a–c**), respiratory exchange ratio (**d–f**), physical activity (**g–i**) and food intake (**j–l**) by weight-cycling mice with or without antibiotic treatment (Abx) during weight loss. Data are from one experiment. Data are mean ± s.e.m. ***$P < 0.01$ by ANOVA. See Supplementary Tables 5 and 6 for exact n and P values.